

BSc Thesis Electrical Engineering

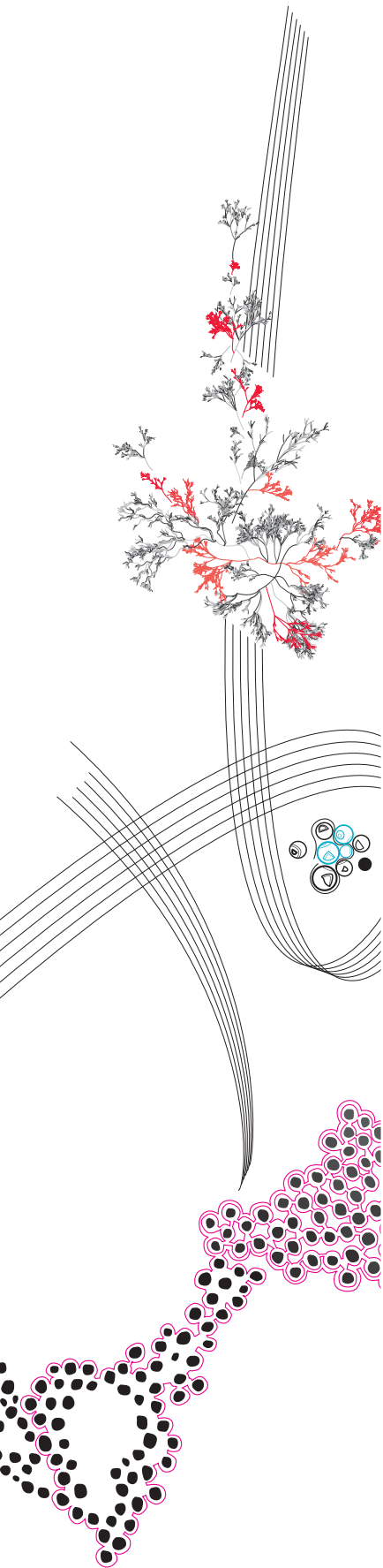
Human Body Blockage Impact on Beamforming

Roy Veld

Committee chair: A.B.J. Kokkeler
Supervisor: A. Alayón Glazunov
External member: P.T. de Boer

July 9, 2021

Faculty of Electrical Engineering,
Mathematics and Computer Science



Abstract — **The impact of the human body blockage on the beamforming performance of a multi-user antenna system is studied. The considered beamforming algorithms are the matched filter (MF) and the zero forcing (ZF) precoding schemes. The body is modelled as an ideal perfect electric conductor (PEC) cylinder. The two users are assumed to be located in the far-field of an access point equipped with a uniform linear array antenna comprised of ideal isotropic radiators separated a half-wavelength apart. Two figures of merit are evaluated: (i) the directivity radiation pattern obtained with the precoding vectors, and (ii) the downlink signal-to-interference-plus noise ratio. As a result of numerical simulations it is observed that the signal attenuation in the direction of the main beam relative the free space (i.e., no blocking body present) depends on the frequency, the number of antennas and the separation distance of the blocking body (i.e., the PEC cylinder). It is observed that at the higher frequency the signal attenuation in the direction of the main beam is larger. Moreover, the higher frequency, the blockage effects become also larger for the larger ULA, as compared to the smaller one, since the elements sense a more uneven field strength.**

I. INTRODUCTION

Antenna systems are becoming increasingly important in everyday life. Over the last decades the use of wireless communication systems employing multiple antennas, i.e., array antennas, has become a vital part of modern day society. The use of multiple-input and multiple-output (MIMO) systems plays a major role in the increasing improvements of nowadays networking systems. In these MIMO systems, beamforming can be implemented. This technique is widely used in wireless communication technology (e.g. 5G and beyond networking systems)[1]. Complex precoding of the beamformer is mostly done at the base station (BS) or the access point (AP) sides of the link. At this side of the link, a human being may be present. A person blocking the incoming or transmitted signal on an antenna may impact communication performance, especially at higher frequencies.

Dozens of studies have been done on the blockage of millimeter waves (mmWaves) by the human body, like the ones in [2] and [3]. Furthermore, some progress has been made previously towards understanding what the blockage impact of a human body is on beamforming[4]. Even though previous research has been done in the past, there is still room for expanding the amount of knowledge. The previous research will be extended.

In this paper, the blockage impact of the human body on the beamforming performance at an access point is studied. The considered beamforming algorithms are the matched filter (MF) and the zero forcing (ZF)

precoding schemes[5]. The analyzed figures of merit are the directivity pattern and the signal-to-interference-plus-noise ratio (SINR). The access point antenna is assumed to be equipped with a uniform linear array (ULA) of ideal isotropic radiating elements separated a half-wavelength apart. No mutual coupling between the antenna elements is considered. The human body is modelled as a perfect electric conductor (PEC) cylinder of infinite extent located at a distance from the array antenna in the broadside direction. The access point serves two users located in the far-field of the array antenna. Hence, the fields scattered by the cylinder are modelled as two plane waves arriving from two different directions perpendicular to the main axis of the cylinder. The MIMO channel matrix of the two-user communication system is computed by superposition of the canonical solution of the plane wave scattering by a PEC cylinder [6].

Two main propagation scenarios are considered in which several parameters have been varied. The first propagation scenario assumes that the plane waves are impinging at the cylinder from two symmetrical directions relative to the broadside direction of the antenna. The second scenario assumes that one plane wave is impinging at the cylinder exactly at the broadside direction of the antenna, while the second wave is impinging at an angle. The above-mentioned figures of merit are computed as a function of the separation angle between the two impinging waves. The computations are repeated for two frequencies, i.e., 1 and 30 GHz, for two separation distances of the cylinder from the array antenna, i.e., 0.5 and 1 m, and various numbers of elements of the array antenna, i.e., 4, 8, 16 and 32. The results are compared with the case when the cylinder is absent, i.e., in free space.

II. SYSTEM MODEL

First, the uplink from both user equipments (UE1 and UE2) to the AP is considered. This is a single-cell, narrowband multi-user MIMO link. The number of single-antenna users is K and the number of AP ULA antenna elements is N . The input-output relationship of the channel is modelled as

$$\mathbf{y} = \sqrt{\text{SNR}}\mathbf{H}\mathbf{x} + \mathbf{n}, \quad (1)$$

where $\mathbf{y} \in \mathbb{C}^{N \times 1}$ is the received signal vector and $\mathbf{x} \in \mathbb{C}^{K \times 1}$ is the transmitted signal vector from both users [5]. The channel matrix is $\mathbf{H} \in \mathbb{C}^{N \times K}$. The noise vector $\mathbf{n} \in \mathbb{C}^{N \times 1}$ describes the additive white Gaussian noise (AWGN) added by the channel. The transmitted signal vector is normalized in power with $E\{\|\mathbf{x}\|^2\} = 1$, where $E\{\|\mathbf{x}\|^2\}$ stands for the expected value of the squared norm of \mathbf{x} .

A. 2D simulation scenario

The ULA consists out of ideal isotropic elements, so the mutual coupling effects between the elements are neglected. A so-called toy model is set up for the simulation scenario. The human body is modelled as a homogeneous, infinite PEC cylinder. The reason for this is a previous study which implies the behavior of the waves scattering off the PEC cylinder approximates the behavior of the ones scattering off a real human body[4]. The advantage of having an infinite cylinder is that the simulation can be done in 2D. A drawing of the simulation scenario is shown in Fig. 1. Two linearly polarized plane waves are incoming at angles φ_1 and φ_2 representing the radiated fields by UE1 and UE2 in far field, respectively. The electric field is pointing in the z-direction, which is the direction perpendicular to the propagation direction of the plane wave. The sum of φ_1 and φ_2 is α . The cylinder is centered in the origin and has radius r . The ULA has N number of elements enumerated as $1, 2, \dots, N$ separated by a distance $d_{el} = \lambda/2$ at the frequency of operation f . The distance between the center of the cylinder and the center of the ULA is D . The angle θ is the angle towards a point in far field with respect to the access point antenna, at which the directivity pattern is evaluated. In the simulation, the total electric field in every

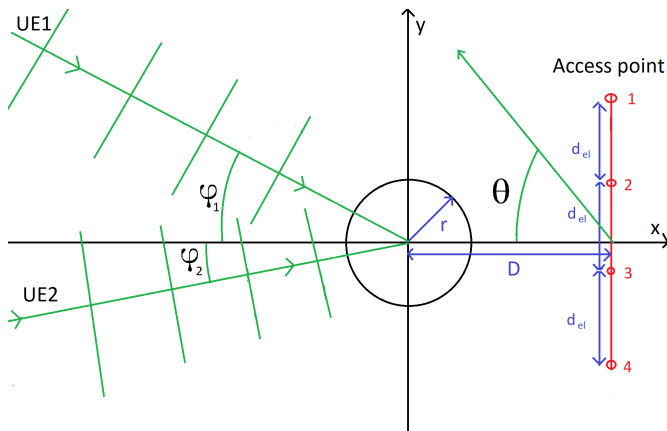


FIG. 1: Sketch of the simulation scenario including parameters.

point in the proximity of the cylinder is computed. The total field is computed as the sum of the incoming plane wave and the waves scattered off the cylinder[7]. Following the assumptions of the toy-model presented above, the channel matrix H is then computed as the total field at the antenna element position due a given user. For example $H_{3,2}$ is the total field at antenna element position 3 due to the impinging field from user 2.

B. Beamforming

As can be seen from (1), the received signal vector at the ULA depends on the channel matrix between the users and the ULA. In order to transmit information from the AP to an UE, the downlink channel matrix $\mathbf{H}_{downlink}$ has to be known. In this study, perfect channel estimation of the uplink channel is assumed as well as perfect channel reciprocity. The electric field is computed by numerical simulations. The downlink channel matrix is then computed as

$$\mathbf{H}_{downlink} = \mathbf{H}_{uplink}^T, \quad (2)$$

where the operation \mathbf{H}_{uplink}^T denotes the transpose of the uplink channel matrix \mathbf{H}_{uplink} . This can be done since the uplink channel and the downlink channels are reciprocal.[8].

Now that the channel state information is known, linear precoding is used to make the antenna form a beam towards the UE. The transmitting signal vector which describes the signals which have to be applied to every single element of the ULA is \mathbf{x} . One could also say that \mathbf{x} is the vector which describes the weighting of every element. The difference with the uplink is that now the signal vector is a N by 1 complex vector instead of a K by 1. With two users, let q_1 and q_2 be the symbols intended for respectively UE1 and UE2. The symbols intended for the two UE's can be put into a vector $\mathbf{q} \in \mathbb{C}^{2 \times 1}$. The relation between \mathbf{x} and \mathbf{q} is

$$\mathbf{x} = \sqrt{\beta} \mathbf{W} \mathbf{q}, \quad (3)$$

where $\mathbf{x} \in \mathbb{C}^{N \times 1}$ is the input signal to the ULA at the AP and the matrix $\mathbf{W} \in \mathbb{C}^{N \times K}$ is the precoding matrix. The factor β normalizes the transmitting vector to make sure the power constraint mentioned above is fulfilled. The normalization factor is given by

$$\beta = \frac{1}{E\{tr(\mathbf{W}\mathbf{W}^H)\}}, \quad (4)$$

where the matrix \mathbf{W} is defined according to the employed precoding scheme.

Two different beamformers are considered

$$\mathbf{W}_{MF} = \mathbf{H}^H \quad (5)$$

and

$$\mathbf{W}_{ZF} = \mathbf{H}^H (\mathbf{H}\mathbf{H}^H)^{-1}, \quad (6)$$

where (5) and (6) are the matched filter (MF) and the zero-forcing (ZF) beamformers. The precoding matrix for MF is obtained by taking the complex conjugate of the channel matrix and is given by (5). The ZF beamformer has a higher computational complexity as can be seen from (6). The two beamformers have different goals. The MF precoding scheme aims to maximize the SNR at the user side, whilst the ZF precoding scheme tries to

suppress interference from other users.[9] The interference of other users can be big while using MF. On the other hand, when using ZF, the noise power can be enhanced.

C. Figures of Merit

In order to quantify the impact of blockage, two figures of merit are computed. The first one is the directivity pattern and the second one is the SINR.

1. Directivity pattern

Every linear array antenna has its own array factor (AF). It is a function of the number of elements, the distance between the elements and the phase and magnitude of the signals applied to the elements. The ULA at the AP has N number of elements which are equally spaced. The array is symmetric in the x -axis with $N/2$ elements on each side of the axis as shown in Fig. 1 for the case of $N = 4$. The array factor for this array configuration is described by

$$AF(\theta) = \sum_{n=1}^N x_n e^{j(\frac{N-(2n-1)}{2})kd_{e1}\sin(\theta)}, \quad (7)$$

where x_n is the signal applied to element n , which is the n th entry of the transmitting vector \mathbf{x} of (3)[10].

The directivity pattern of an antenna can be evaluated as a function of angle θ , i.e., the direction of radiation

$$D_{ant}(\theta) = \left| \frac{U(\theta)}{U_0} \right|, \quad (8)$$

where the radiation intensity $U(\theta)$ is given by

$$U(\theta) = [AF(\theta)]^2, \quad (9)$$

and U_0 is the average radiation intensity and can be computed as

$$\begin{aligned} U_0 &= \frac{1}{4\pi} \int_0^{2\pi} \int_{-\pi/2}^{\pi/2} |U(\theta)| \cos(\theta) d\theta d\phi \\ &= \frac{1}{2} \int_{-\pi/2}^{\pi/2} |U(\theta)| \cos(\theta) d\theta. \end{aligned} \quad (10)$$

In other words, U_0 is the total radiation intensity that would be radiated by an ideal isotropic antenna with equal intensity over all directions, i.e., evenly over the sphere of unit radius[11]. In (7), (8), (9) and (10), θ is the angle described in Fig. 1. This means $\theta = 0$ corresponds to the broadside direction of the array ϕ is the azimuth angle.

In order to evaluate the impact of the user body modelled by the PEC cylinder on the far-field directivity pattern of the array we define the beamforming directivity loss (BFDL)

$$L_{\text{BFD}}(\alpha) = 10 \log \left(\frac{D_{\text{max}}(\alpha)}{D_{\text{ref}}(\alpha)} \right), \quad (11)$$

where $D_{\text{max}}(\alpha) = \max\{D_{\text{ant}}(\theta, \alpha)\}$, and $D_{\text{ref}}(\alpha) = \max\{D_{\text{ant,ref}}(\theta, \alpha)\}$ are the maximum of the computed directivity pattern at each angle α in the presence of the human body (i.e., PEC cylinder) and in its absence (i.e., free space), respectively. Then, we compute the maximum of (11) $L_{\text{BFD,max}} = \max\{L_{\text{BFD}}(\alpha)\}$ and the angle α_{max} at which it occurs. Similarly we compute the minimum of (11) $L_{\text{BFD,min}} = \min\{L_{\text{BFD}}(\alpha)\}$ and the angle α_{min} at which it occurs. The parameters $L_{\text{BFD,max}}$ and $L_{\text{BFD,min}}$ evaluate the variation of the directivity in the main beam of the far-field directivity pattern as the result of the presence of the human body. Results will be computed for the different scenarios and parameters.

2. SINR

The per-user received signal-to-interference-plus-noise ratio (SINR) is a fundamental parameter to quantify the quality of wireless communication systems. This ratio, which is different from the SNR, also takes interference from other signals into account. The received SINR of the user k can be computed by

$$\text{SINR}_k = \frac{\beta \text{SNR} |\mathbf{H}_k: \mathbf{W}_k|^2}{\beta \text{SNR} \sum_{k' \neq k}^K |\mathbf{H}_k: \mathbf{W}_{k'}|^2 + 1}, \quad (12)$$

where \mathbf{H}_k is the k th row of matrix \mathbf{H} and \mathbf{W}_k is the k th column of the matrix \mathbf{W} . β is the normalization factor found in (4). Here, K is the number of interfering users. Since there is only one interfering user in this research, (12) can be simplified to

$$\text{SINR}_k = \frac{\beta \text{SNR} |\mathbf{H}_k: \mathbf{W}_k|^2}{\beta \text{SNR} |\mathbf{H}_k: \mathbf{W}_{k'}|^2 + 1}, \quad (13)$$

where $k' \neq k$. In the fraction, the numerator defines the received signal power of the signal of interest. The denominator defines the sum of the interference power and noise power.

Furthermore, in order to evaluate the impact of the user body modelled by the PEC cylinder on the per-user SINR, we compute the per-user SINR loss at a fixed SNR value and angle α

$$L_{\text{SINR},k}(\alpha, \text{SNR}) = 10 \log \left(\frac{\text{SINR}_k(\alpha, \text{SNR})}{\text{SINR}_k^{\text{ref}}(\alpha, \text{SNR})} \right), \quad (14)$$

where SINR_k and $\text{SINR}_k^{\text{ref}}$ are the per-user SINR in the presence of the human body (i.e., PEC cylinder) and in

its absence (i.e., free space), respectively. Then, we compute the maximum of (14) $L_{\text{SINR,max}} = \max\{L_{\text{SINR}}(\alpha)\}$ for a given SNR value and the angle α_{max} at which it occurs. It is worthwhile to note that we have dropped the index "k" for the sake of compactness. Similarly we compute the minimum of (14) $L_{\text{SINR,min}} = \min\{L_{\text{SINR}}(\alpha)\}$ and the angle α_{min} at which it occurs. The parameters $L_{\text{SINR,max}}$ and $L_{\text{SINR,min}}$ evaluate the variation of the per-user SINR as the result of the presence of the human body. Results will be computed for the different scenarios and parameters.

III. SIMULATION RESULTS AND ANALYSIS

The scenario is simulated using a modified MATLAB code for a plane wave scattering on a cylinder made by G. Kevin Zhu.[7] In this MATLAB code, several parameters can be set. The (variable) parameters and the values for which the simulations are done can be seen in Table I. The simulations with the different parameters will be done for two cases:

- Case I is the case where the impinging plane waves are coming in from directions relative to the broadside direction of the array defined by the angles $\varphi_{1,2} \in \pm[0.5^\circ \ 60^\circ]$. Here, $\alpha \in [1^\circ \ 120^\circ]$.
- Case II is the case where one wave is always coming in at broadside direction ($\varphi_2 = 0^\circ$) and the second wave is coming from angle $\varphi_1 \in [0.5^\circ \ 60^\circ]$ relative to the broadside direction. Here, $\alpha \in [0.5^\circ \ 60^\circ]$.

The existing MATLAB code also allows plotting the electric field of the impinging plane waves. This is done in Fig. 2 to visualise the simulation scenario. The red dots in each plot are the elements of the ULA.

Since we assume ideal isotropic antennas with no mutual coupling, we compute the electric field in the points where the antenna elements are located. When the electric field in the elements are known the downlink channel matrix can be computed and the precoding matrix can be obtained. For now the other points around the cylinder are also computed and plotted, only for visualizing the electric field and clarifying the simulation scenario.

TABLE I: Simulation parameters. See Fig. 1 for the geometrical parameter definition.

Parameter	Value
cylinder radius r	15 cm
inter-element distance d_{el}	$\lambda/2$ m
frequency f	{1 GHz, 30 GHz}
separation angle α	$[1^\circ \dots 120^\circ]$ (symmetric) $[1^\circ \dots 60^\circ]$ (non-symmetric)
number of elements N	{4, 8, 16, 32}
ULA-cylinder distance D	{0.5 m, 1.0 m}

A. Directivity pattern

For all angles α showed in Table I, the directivity pattern is computed. All radiation patterns from -90° to 90° are plotted for every value of α .

A 2D surface plot is a clear way to plot the radiation patterns for all different angles of α . The magnitude of the directivity pattern is displayed by using a color scale. The directivity is given in linear scale. This is a unitless quantity. First, only the plots for Case I are plotted and analyzed. Secondly, the same is done for the plots in case II.

In order to be able to show what the influence of the cylinder (human body) is on the beamforming performance of the antenna, the simulations were also done for the situation where there is no cylinder. Subsequently, the outcome of the simulations with and without cylinder can be compared.

1. Directivity Case I

The directivity 2D surface plots in the symmetric Case I for $N = 4$ and $N = 32$ at 1 GHz are shown in Figs. 3 and 4, respectively. Corresponding results at 30 GHz are given in Figs. 5 and 6, respectively. In order to reduce the number of figures, only the plots for $N = 4$ and $N = 32$ are presented because the ones for $N = 8$ and $N = 16$ show similar trends. When increasing the number of elements, the beam becomes narrower and the magnitude of the beam becomes higher. Only the directivity from UE1 is plotted because the plots for UE2 are exactly the same plot as for UE1, but mirrored at $\theta = 0$.

When comparing the directivity plots with and without the cylinder for $D = 0.5$ m at 1 GHz in Fig. 3, several observations can be made. For example, compare Fig. 3a with Fig. 3c showing the directivity pattern for the MF beamforming, with and without the cylinder, respectively. As can be seen from Fig. 3a, for $N=4$, the angle of maximum directivity does not always coincides with the angle where the UE is located. The main lobe often deviates from the line-of-sight radiation. This is most clearly the case for $\alpha < 80^\circ$. Furthermore, as can be seen from Fig. 3c, in free space, the main beam is always directed towards the UE. Hence, the cylinder is clearly blocking the incoming signal at values of $\alpha < 80^\circ$. When performing the MF precoding the beam is not formed towards the line-of-sight direction towards the user because of the blocking attenuation. Instead, beams are pointed towards directions of the scattered field.

With ZF precoding (Fig. 3d-f), the results are somewhat similar. However, the most important is to look

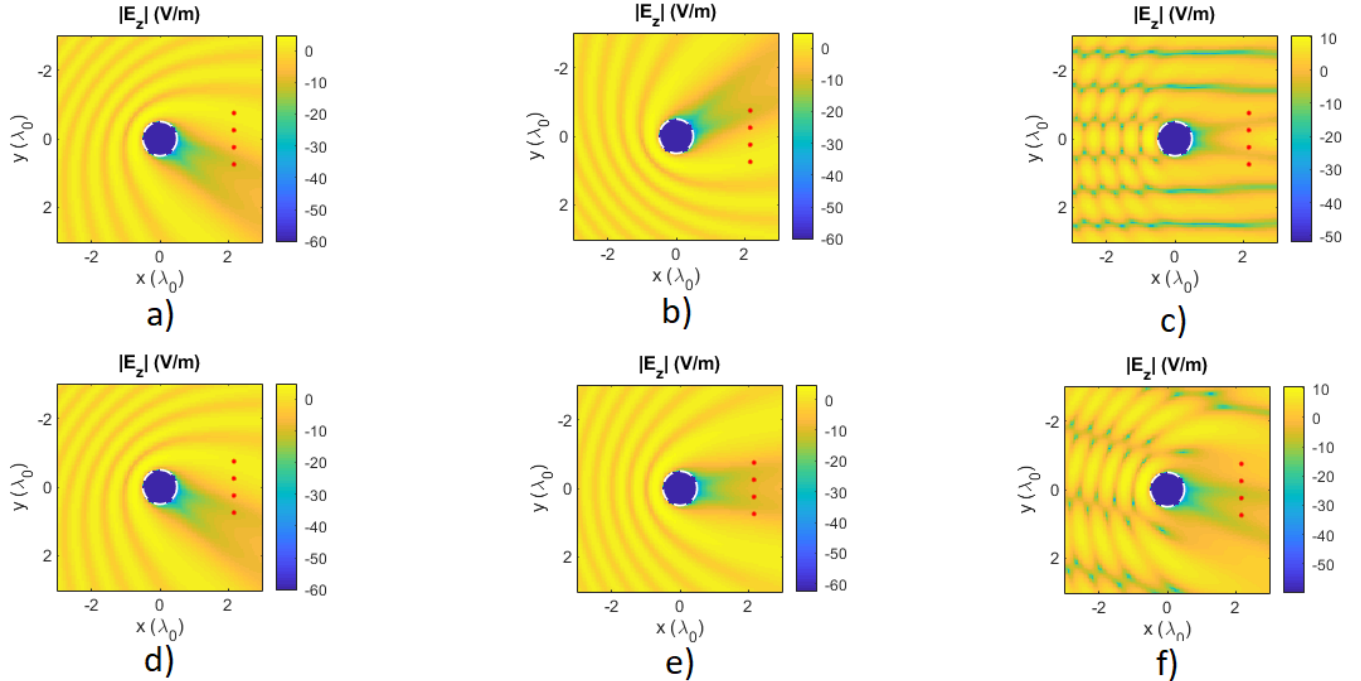


FIG. 2: Plane waves scattering off the cylinder. Figures a) to c) are for case I. Figures d) to f) are for case II. The wave from UE1 is shown in plots a) and d). The one from UE2 is seen in b) and e). The sum of the two waves can be seen in figures c) and f) for respectively Case I and case II. $f = 1\text{GHz}$, $N = 4$ and $D = 0.5\text{m}$. The angle of arrival with respect to the broadside direction in the plots is $\pm 30^\circ$ for case I. For case II, this is 30° for UE1 and 0° for UE2.

in the direction of the "main null" of the directivity pattern, i.e., the line towards the direction of UE2. The difference is that around $\alpha = 30^\circ$ the magnitude of the main lobe is lower when compared to the free space line-of-sight simulation. At for example $\alpha = 27^\circ$, for $D = 0.5\text{ m}$ the directivity is attenuated by 3.4 dB. A possible reason for this is the blocking effect being higher for the ZF algorithm in terms of the radiated power towards the UE since the the ZF algorithm does not maximize power, but minimizes interference. Moreover, it is clear from the figures that when the distance D gets lower, even less energy is received around $\alpha = 30^\circ$.

Furthermore, when comparing the simulations for $D = 0.5\text{ m}$ and $D = 1\text{ m}$ it is clearly visible that for the lower separation distance (Figs. 3a and 3d) the magnitude of the directivity is lower at small angles of α . For the case of matched filter, which is shown in Fig. 3a, the directivity loss for $\alpha < 70^\circ$ can get as high as 1.8 dB. When looking at Fig. 3b, the directivity loss at $\alpha < 60^\circ$ can get to at most 1.0 dB. These results can be explained by looking at Fig. 2a-c. It illustrates the case where $\alpha = 60^\circ$. It becomes clear there are certain areas where destructive interference occurs. When this is precisely the case at the location of an antenna element, the power this element receives is low.

Fig. 4 shows similar results as in Fig. 3, but for $N=32$. However, when comparing the figures without the cylinder Fig. 4c and Fig. 4f to the other ones which have a cylinder, what stands out is the magnitude of the line of maximum directivity, which is 14.2 dBi at its lowest. This is slightly lower than the directivity of 15.05 dBi when there is a cylinder. Therefore, the directivity loss can get up to 0.85 dB. When there is no cylinder the maximum directivity is equal to the number of elements ($D_{ant,max} = N$). Furthermore, the plots which include a cylinder (Fig. 4a, b, d, e) have a sidelobe magnitude which is considerably higher than without the cylinder. The reason for this is the relatively big number of antenna elements. The antenna has 32 elements, so it becomes 4.65 meters in total size. Compared to the cylinder size of 15 cm, this is large. Therefore the cylinder does not have a lot of influence on the directivity of the antenna, except for adding some additional sidelobes for some values of α . The additional sidelobes result in a lower magnitude of the main lobe (14.2 dBi) since the radiated power is more spread out to different angles.

Fig. 5 shows similar plots to Fig. 3, but now $f = 30\text{ GHz}$. Now we compare Figs. 5a and 5b with Figs. 3a and 3b. For a frequency of 30 GHz, at separation angles $\alpha < 20^\circ$, the main beam direction oscillates faster compared to the results of 1 GHz. Furthermore, with

$f = 30$ GHz the directivity loss is approximately 1.6 dB and 0.8 dB for values of D of 0.5 m and 1 m, respectively. In Figs. 5d and 5e the plots closely corresponds to the plot without the cylinder shown in Fig. 5f. A possible reason for the change in radiation pattern plots with respect to the case without cylinder are the dimensions of the objects in the simulation. For the cylinder the dimensions are fixed, while the frequency changes. With a higher frequency the size of the ULA changes. The separation distance between the elements is $\lambda/2$. With $N = 4$ and $f = 1$ GHz, the total size of the array is 45 cm. When having a higher frequency of 30 GHz, the total size of the array is 1.5 cm. Only for $\alpha < 20^\circ$ the directivity plot of the 30 GHz case is not the same as the non-cylinder case. This can be explained by the fact that here the cylinder is exactly in the line of sight between the antenna elements and the UE. At larger angles of arrival ($\alpha > 20^\circ$), the scattering of the incoming wave on the cylinder does not have influence on the electric field seen in the antenna elements. In this case the line-of-sight is not fully obstructed. At the frequency of 1 GHz the size of the ULA is higher and the plane wave which is altered significantly by the cylinder reaches the elements. Due to the size of the ULA, often the cylinder is blocking the line of sight of at least one element towards the UE.

Fig. 6 shows similar results as in Fig. 4, but for $f = 30$ GHz. When having a high number of elements ($N = 32$) and a high frequency ($f = 30$ GHz), the directivity is only attenuated at low angles of α . The magnitude of the directivity is low for a wider range of separation angles when having a lower D . For $D = 1$ m there is an attenuation in directivity only for $\alpha < 10^\circ$. For $D = 0.5$ m this range extends to $\alpha < 25^\circ$. For a separation distance D of 0.5 m the range of α being affected by the cylinder is more than twice as big as for the case of $D = 1$ m. The closer the ULA is to the cylinder, the more impact the cylinder has on the beamforming of the ULA at $f = 30$ GHz and $N = 32$. For both values of D , with a lower α the attenuation gets bigger. For some angles the magnitude of the directivity loss can get as high as 5.0 dB. This is because of the ULA being closer to the cylinder and therefore less elements have a free line of sight towards the UE. By increasing the angle of arrival at some point all elements have a direct line of sight towards the UE.

In case of having no cylinder next to the antenna, the frequency of operation does not matter for the directivity pattern of the antenna. The whole antenna scales with the frequency because $d_{el} = \lambda/2$. The electrical behavior of the antenna is exactly the same as expected.

The minimum and the maximum of the beamforming directivity loss and the corresponding α angles at which they occur are summarized in Table II for Case I and 1 GHz. The corresponding results for 30 GHz are given in Table III.

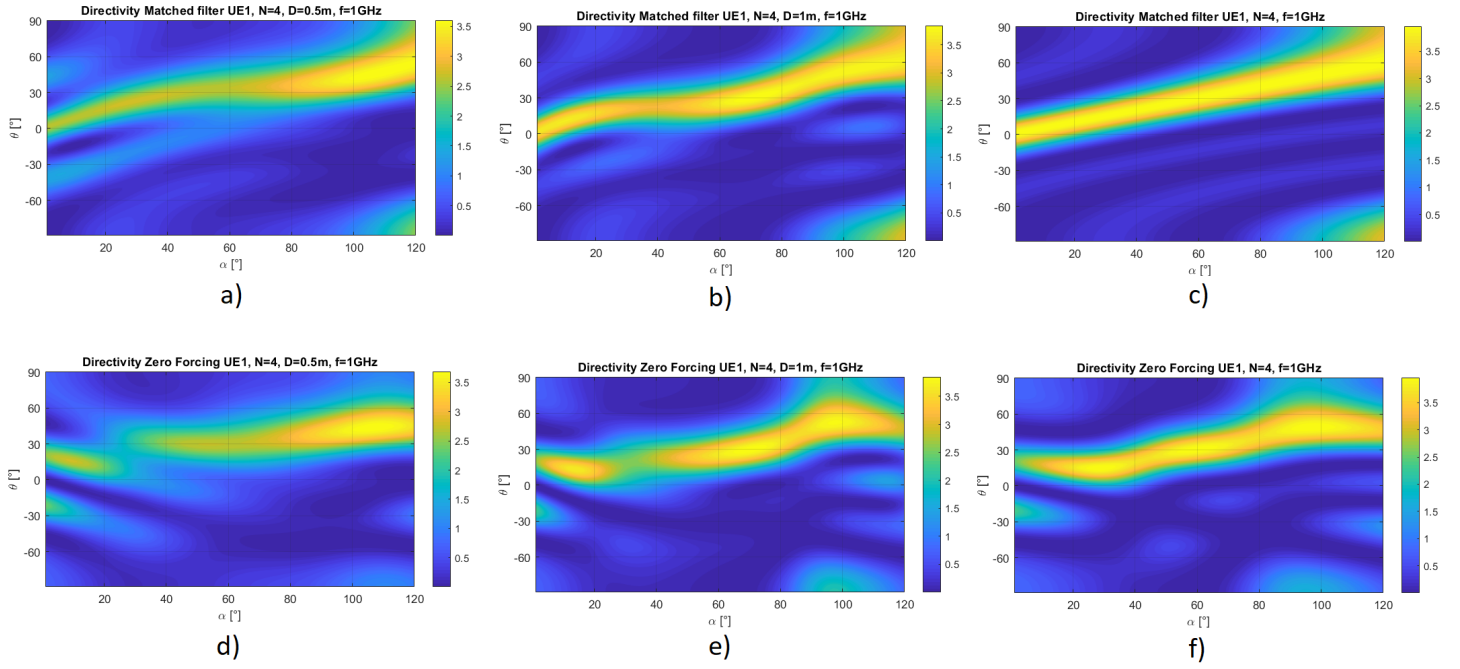


FIG. 3: 2D surface plots of the directivity pattern for $N = 4$ and $f = 1\text{GHz}$ in case I. From left to the right, the three columns represent respectively $D = 0.5\text{ m}$, $D = 1\text{ m}$ and no cylinder. Plots a)-c) are MF plots and d)-f) are ZF plots. All plots are in linear scale.

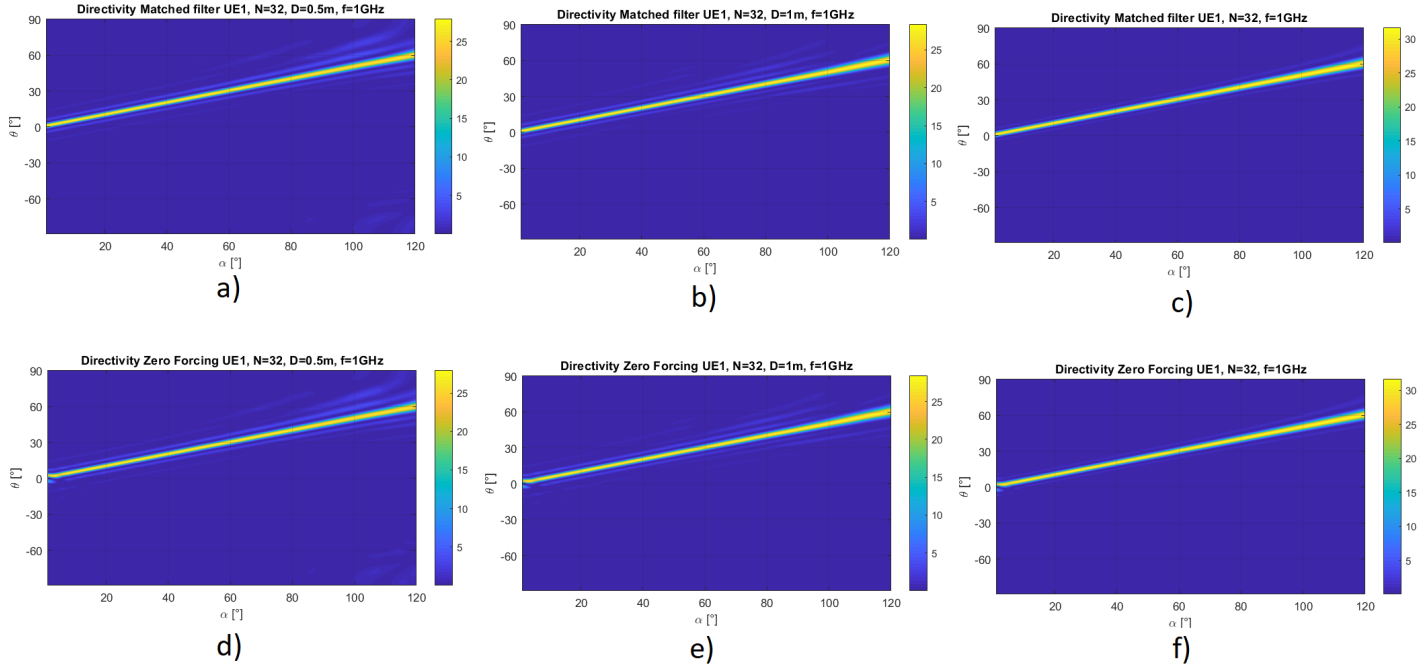


FIG. 4: 2D surface plots of the directivity pattern for $N = 32$ and $f = 1\text{ GHz}$ in case I. From left to the right, the three columns represent respectively $D = 0.5\text{ m}$, $D = 1\text{ m}$ and no cylinder. Plots a)-c) are MF plots and d)-f) are ZF plots. All plots are in linear scale.

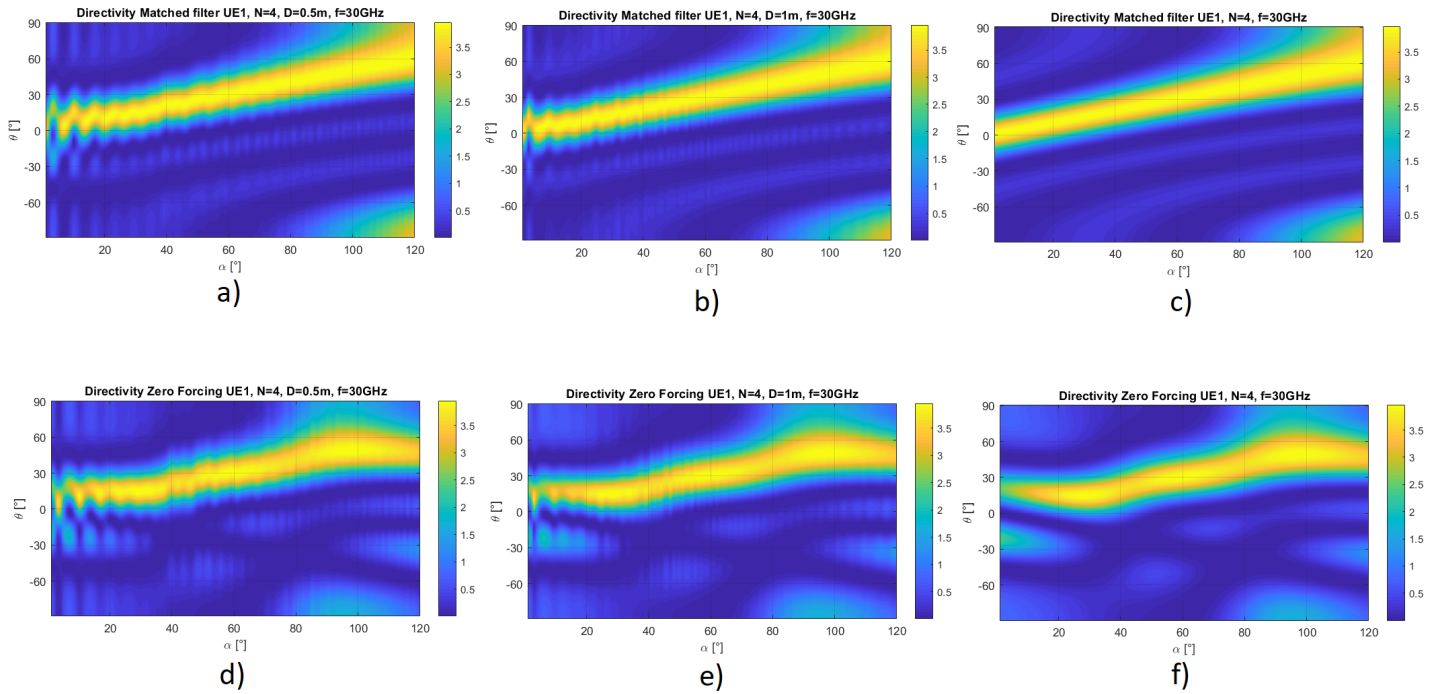


FIG. 5: 2D surface plots of the directivity pattern for $N = 32$ and $f = 30$ GHz in case I. From left to the right, the three columns represent respectively $D = 0.5$ m, $D = 1$ m and no cylinder. Plots a)-c) are MF plots and d)-f) are ZF plots. All plots are in linear scale.

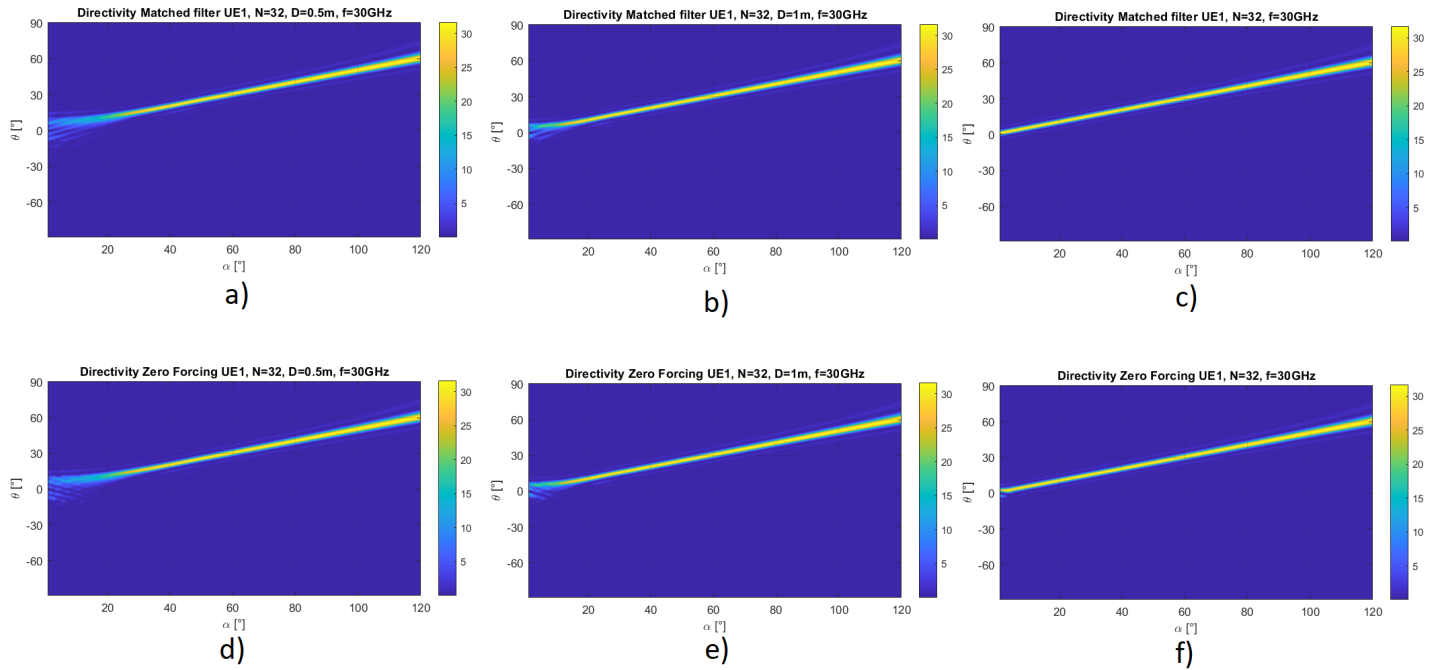


FIG. 6: 2D surface plots of the directivity pattern for $N = 32$ and $f = 30$ GHz in case I. From left to the right, the three columns represent respectively $D = 0.5$ m, $D = 1$ m and no cylinder. Plots a)-c) are MF plots and d)-f) are ZF plots. All plots are in linear scale.

TABLE II: Beamforming directivity loss for UE1 (same for UE2) Case I at 1 GHz.

		MF						ZF			
		$L_{\text{BFDL},\text{min}}$ [dB]	$\alpha_{\text{min}} [^\circ]$	$L_{\text{BFDL},\text{max}}$ [dB]	$\alpha_{\text{max}} [^\circ]$			$L_{\text{BFDL},\text{min}}$ [dB]	$\alpha_{\text{min}} [^\circ]$	$L_{\text{BFDL},\text{max}}$ [dB]	$\alpha_{\text{max}} [^\circ]$
N=4	D=0.5 m	-1.8	1	-0.4	108	D=0.5 m	-3.4	27	0.0	1	
	D=1 m	-1.0	38	-0.1	72	D=1 m	-1.9	31	0.5	8	
N=8	D=0.5 m	-1.8	55	-0.9	120	D=0.5 m	-4.2	23	-0.5	1	
	D=1 m	-1.3	22	-0.3	108	D=1 m	-3.0	21	-0.1	107	
N=16	D=0.5 m	-1.2	103	-0.9	15	D=0.5 m	-1.5	10	-0.2	1	
	D=1 m	-0.8	21	-0.4	120	D=1 m	-1.5	10	-0.2	1	
N=32	D=0.5 m	-0.8	120	-0.5	1	D=0.5 m	-0.8	113	-0.2	1	
	D=1 m	-0.6	101	-0.5	1	D=1 m	-0.7	5	-0.2	1	

TABLE III: Beamforming directivity loss for UE1 (same for UE2) Case I at 30 GHz.

		MF						ZF			
		$L_{\text{BFDL},\text{min}}$ [dB]	$\alpha_{\text{min}} [^\circ]$	$L_{\text{BFDL},\text{max}}$ [dB]	$\alpha_{\text{max}} [^\circ]$			$L_{\text{BFDL},\text{min}}$ [dB]	$\alpha_{\text{min}} [^\circ]$	$L_{\text{BFDL},\text{max}}$ [dB]	$\alpha_{\text{max}} [^\circ]$
N=4	D=0.5 m	-1.6	2	0	92	D=0.5 m	-0.5	5	1.3	3	
	D=1 m	-0.8	4	0	22	D=1 m	-0.2	18	1.5	3	
N=8	D=0.5 m	-2.4	1	0	117	D=0.5 m	-1.5	11	0.3	7	
	D=1 m	-1.2	4	0	120	D=1 m	-0.3	5	1.4	3	
N=16	D=0.5 m	-3.1	2	0	120	D=0.5 m	-2.6	7	0	118	
	D=1 m	-2.0	1	0	116	D=1 m	-2.2	4	0.3	1	
N=32	D=0.5 m	-5.0	1	0	116	D=0.5 m	-4.9	3	0	119	
	D=1 m	-4.0	2	0	120	D=1 m	-2.7	1	0	120	

2. Directivity Case II

After treating Case I where the waves were coming in symmetrically, the directivity pattern 2D surface plots for Case II were plotted. In case II, one wave is coming in from broadside (UE2) and the other one from a variable angle (UE1). The plots of UE1 are similar to the plots of UE1 in Case I so these are not plotted again. The angle of UE1, φ_1 , is exactly the same for both cases I and II. The directivity 2D surface plots for UE2 with $N = 4$ and $f = 1$ GHz are shown in Fig. 7. Directivity plots with $N = 32$ and $f = 30$ GHz for Case II are shown in Fig. 8.

As can be seen from Fig. 7a-c the sidelobes increase with lower distance between cylinder and antenna. Higher side lobes magnitude means less power is radiated in the main beam. For $D = 0.5$ m the sidelobe magnitude in Fig. 7a is 1.4 (1.5 dBi). For $D = 1$ m the magnitude of the sidelobes in Fig. 7b is already 0.4 (-4.0 dBi). The main beam is at $\theta = 0^\circ$ with a directivity attenuation of 1.8 dB and 0.4 dB for $D = 0.5$ m and $D = 1$ m, respectively. This behavior can be explained by the scattering of the incoming wave off the cylinder. Since the incoming wave is coming from UE2 at an angle of $\theta = 0^\circ$, the cylinder is exactly in between the transmitting and receiving antenna. This can be further understood by inspecting Fig. 2e. The magnitude of the electric field is low on the opposite side of where the plane wave is coming from. However, when moving further away from the cylinder the magnitude of the electric field increases again. When the ULA is closer to the cylinder the blockage effect is higher. The sidelobes increase because the ULA is receiving power from angles other than $\theta = 0^\circ$ as well. This is because of the scattered waves. For example, in Fig. 7a and 7b there are sidelobes between $\theta = \pm 30^\circ$ and $\theta = \pm 60^\circ$. The antenna receives power from these angles as well even though the main power only comes from one specific angle.

For plots 7d-f the magnitude of the sidelobe which is present at $\alpha < 10^\circ$ is higher for $D = 0.5$ m as well. The zero forcing scheme works such that it puts a null on the interfering UE, while it still needs to radiated power at the desired user. Due to a low number of antenna elements this is not possible because the sidelobes are large and the directivity of UE1 and UE2, when they are close to each other, can not be maximized and nulled respectively at the same time.

As can be seen from the plots in Fig. 8a,b,d,e for $N = 32$ the beamformers can not succeed to focus the transmit power towards the broadside direction because there is a cylinder in the line-of-sight. Multiple small beams are formed to angles just above and below $\theta = 0$. The maximum directivity attenuation with respect to the free space case for the matched filter is 5.5 dB

and 3.5 dB at $D = 0.5$ m and $D = 1$ m, respectively. Because of the cylinder blocking the incoming signal, the electric field at the ULA elements does not come from the broadside direction. The ULA receives the waves at approximately $\theta = \pm 10^\circ$. The beamwidth of the two beams increases with a lower distance D . With a wider beam, there is a lower maximum directivity. Power is received from a wider range of angles θ . Because of the ULA being closer to the cylinder, it looks like the signal is coming in from a range of different angles.

The minimum and the maximum of the beamforming directivity loss and the corresponding α angles at which they occur are summarized in Table IV and Table V, for UE1 and UE 2, respectively, for Case II and 1 GHz. The corresponding results for 30 GHz are given in Table VI and Table VII.

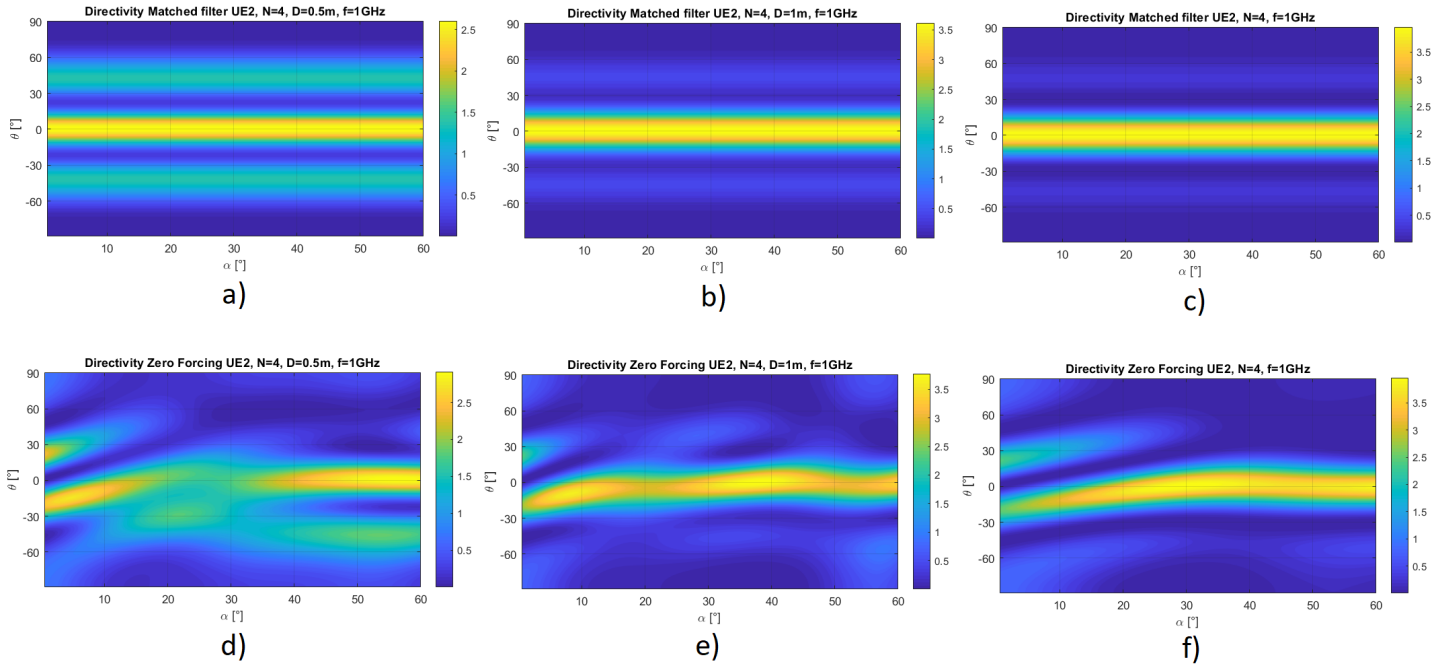


FIG. 7: 2D surface plots of the directivity pattern for $N = 4$ and $f = 1$ GHz in case II. From left to the right, the three columns represent respectively $D = 0.5$ m, $D = 1$ m and no cylinder. Plots a)-c) are MF plots and d)-f) are ZF plots. The plot are made for UE2 which is located at broadside of the antenna. All plots are in linear scale.

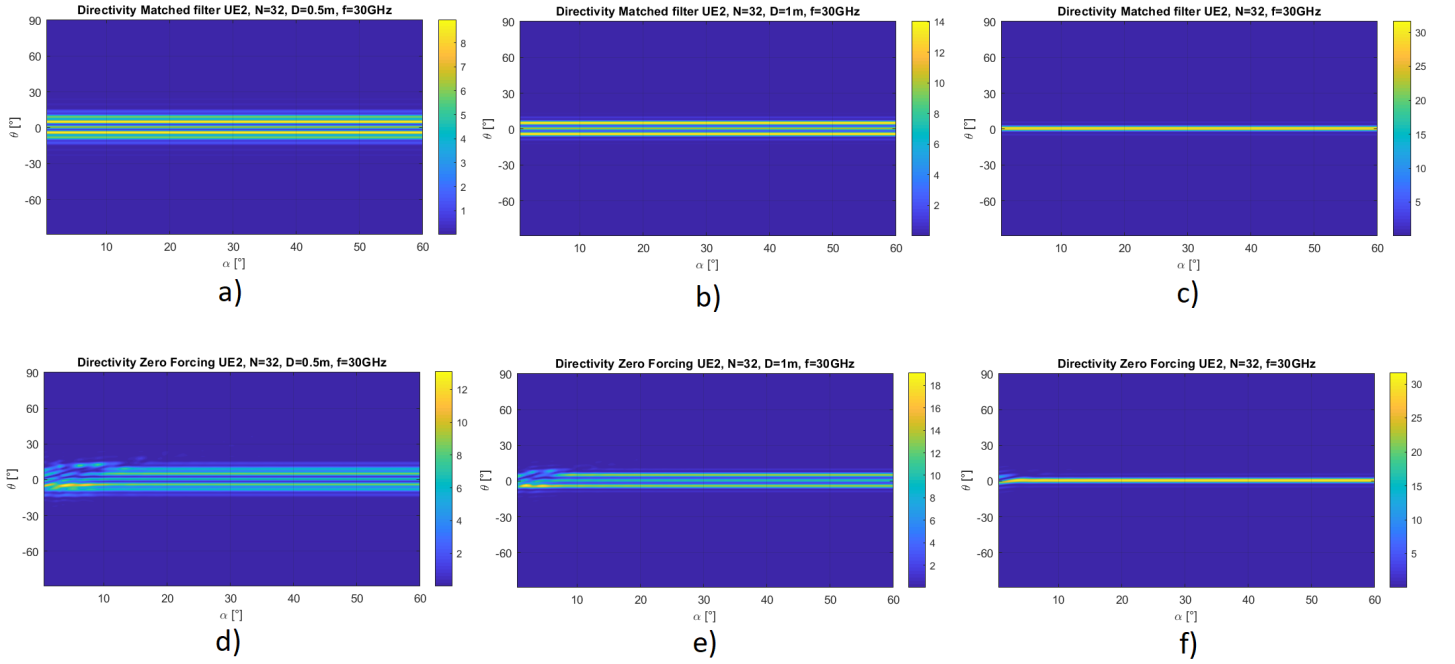


FIG. 8: 2D surface plots of the directivity pattern for $N = 32$ and $f = 30$ GHz in case II. From left to the right, the three columns represent respectively $D = 0.5$ m, $D = 1$ m and no cylinder. Plots a)-c) are MF plots and d)-f) are ZF plots. The plot are made for UE2 which is located at broadside of the antenna. All plots are in linear scale.

TABLE IV: Beamforming directivity loss for UE1, Case II at 1 GHz.

		MF				ZF				
		$L_{\text{BFDL,min}}$ [dB]	$\alpha_{\text{min}} [^\circ]$	$L_{\text{BFDL,max}}$ [dB]	$\alpha_{\text{max}} [^\circ]$	$L_{\text{BFDL,min}}$ [dB]	$\alpha_{\text{min}} [^\circ]$	$L_{\text{BFDL,max}}$ [dB]	$\alpha_{\text{max}} [^\circ]$	
N=4	D=0.5 m	-1.8	0.5	-0.4	54	D=0.5 m	-2.0	54.5	0	0.5
	D=1 m	-1.0	19	-0.1	36	D=1 m	-0.5	14.5	0	0.5
N=8	D=0.5 m	-1.8	27.5	-0.9	60	D=0.5 m	-3.4	21	-0.4	0.5
	D=1 m	-1.3	11	-0.3	54	D=1 m	-2.3	19	-0.2	0.5
N=16	D=0.5 m	-1.2	51.5	-0.9	7.5	D=0.5 m	-1.6	10.5	-0.1	0.5
	D=1 m	-0.8	10.5	-0.4	60	D=1 m	-1.5	10	-0.1	0.5
N=32	D=0.5 m	-0.8	60	-0.5	0.5	D=0.5 m	-0.8	0.5	-0.1	0.5
	D=1 m	-0.6	50.5	-0.5	0.5	D=1 m	-0.7	0.5	-0.1	0.5

TABLE V: Beamforming directivity loss for UE2, Case II at 1 GHz.

		MF				ZF				
		$L_{\text{BFDL,min}}$ [dB]	$\alpha_{\text{min}} [^\circ]$	$L_{\text{BFDL,max}}$ [dB]	$\alpha_{\text{max}} [^\circ]$	$L_{\text{BFDL,min}}$ [dB]	$\alpha_{\text{min}} [^\circ]$	$L_{\text{BFDL,max}}$ [dB]	$\alpha_{\text{max}} [^\circ]$	
N=4	D=0.5 m	-1.8	all	-1.8	all	D=0.5 m	-3.7	27.5	0.1	2
	D=1 m	-0.4	all	-0.4	all	D=1 m	-1.1	22.5	0.9	5.5
N=8	D=0.5 m	-1.6	all	-1.6	all	D=0.5 m	-3.5	20.5	-0.4	0.5
	D=1 m	-1.2	all	-1.2	all	D=1 m	-2.5	18.5	-0.2	0.5
N=16	D=0.5 m	-1.0	all	-1.0	all	D=0.5 m	-1.6	10.5	-0.1	0.5
	D=1 m	-0.8	all	-0.8	all	D=1 m	-1.4	10	-0.1	0.5
N=32	D=0.5 m	-0.5	all	-0.5	all	D=0.5 m	-0.8	5	-0.1	0.5
	D=1 m	-0.5	all	-0.5	all	D=1 m	-0.7	5	-0.1	0.5

TABLE VI: Beamforming directivity loss for UE1, Case II at 30 GHz.

		MF				ZF				
		$L_{\text{BFDL,min}}$ [dB]	$\alpha_{\text{min}} [^\circ]$	$L_{\text{BFDL,max}}$ [dB]	$\alpha_{\text{max}} [^\circ]$	$L_{\text{BFDL,min}}$ [dB]	$\alpha_{\text{min}} [^\circ]$	$L_{\text{BFDL,max}}$ [dB]	$\alpha_{\text{max}} [^\circ]$	
N=4	D=0.5 m	-1.6	1	0	47	D=0.5 m	-0.6	11.5	0.2	47
	D=1 m	-0.8	2	0	11	D=1 m	-0.3	7.5	0.1	44.5
N=8	D=0.5 m	-2.4	0.5	0	58.5	D=0.5 m	-1.8	11	0.1	0.5
	D=1 m	-1.2	2	0	60	D=1 m	-0.6	5	0.2	20
N=16	D=0.5 m	-3.1	1	0	60	D=0.5 m	-4.6	4	0	16.5
	D=1 m	-2.0	0.5	0	58	D=1 m	-1.8	4.5	0	12.5
N=32	D=0.5 m	-5.0	0.5	0	58	D=0.5 m	-5.3	3.5	0	54.5
	D=1 m	-4.0	1	0	60	D=1 m	-4.7	2	0	54.5

TABLE VII: Beamforming directivity loss for UE2, Case II at 30 GHz.

		MF				ZF					
		$L_{\text{BFDL,min}}$ [dB]	$\alpha_{\text{min}} [^\circ]$	$L_{\text{BFDL,max}}$ [dB]	$\alpha_{\text{max}} [^\circ]$			$L_{\text{BFDL,min}}$ [dB]	$\alpha_{\text{min}} [^\circ]$	$L_{\text{BFDL,max}}$ [dB]	$\alpha_{\text{max}} [^\circ]$
N=4	D=0.5 m	-0.1	23	-0.1	8	D=0.5 m	-0.2	2.5	1.5	1.5	
	D=1 m	0	54.5	0	35	D=1 m	-0.1	51.5	1.6	1.5	
N=8	D=0.5 m	-3.1	4.5	-3.1	34	D=0.5 m	-3.1	48	1.0	3.5	
	D=1 m	-0.1	27	-0.1	49.5	D=1 m	-0.2	23	1.9	1.5	
N=16	D=0.5 m	-2.8	11	-2.8	58	D=0.5 m	-2.9	34.5	-0.2	2	
	D=1 m	-3.2	54.5	-3.2	9.5	D=1 m	-3.2	12.5	0.7	0.5	
N=32	D=0.5 m	-5.5	20	-5.5	11.5	D=0.5 m	-5.5	13.5	-3.0	0.5	
	D=1 m	-3.5	7	-3.5	34	D=1 m	-3.6	15.5	-1.4	1.5	

B. SINR plots

Next, 2D surface plots of the SINR are produced as a function of the separation angle α given in Table I and as function of the signal-to-noise ratio for SNR = $[-10 \text{ dB}, \dots, 30 \text{ dB}]$. As above, we consider the cases I and II.

1. SINR Case I

The SINR surface plots in Case I are always the same for both UE1 and UE2. The reason for this is the locations of the users being symmetric with respect to the antenna and the cylinder. Therefore, when looking at UE2 as interferer and UE1 as desired signal or vice versa, either way the SINR is always the same. This is because both incoming waves are the exact same linearly polarized plane waves, only with an angle of arrival of opposite sign. In the plots for Case I only the plots for UE1 are shown. Just like the plots for the directivity, the plots for $f = 1 \text{ GHz}$ and $f = 30 \text{ GHz}$ are exactly the same when there is no cylinder in the proximity of the ULA.

In Fig. 9 the SINR is plotted for $N = 4$ with MF precoding. All five subfigures in this figure have 3 peaks at certain values of α for high SNR. The value for α at where the peaks occur is different for every simulation scenario. However, to some extent there is a pattern in the regions in which the peaks occur. When the separation distance D between the cylinder and the antenna changes, the angles where the peaks are located change slightly. At low SNR (lower than 5 dB), there are no peaks visible. In case of having a cylinder next to the antenna, the SINR for low SNR increases with a higher separation angle α . The reason for this is when the plane waves are coming in too closely together, they have more interference with each other. This will increase the interference power and therefore the SINR is lower. What can also play a role here is the received power from the wanted signal being low because the plane wave is scattered by the cylinder.

All SINR plot shows minima and maxima. In order to understand the origin of these peaks and valleys in SINR, the directivity plots for UE1 and UE2 at a value of α at which a peak, or a valley, occurs are shown next. For example, in Fig. 9e a peak occurs at $\alpha = 29^\circ$, and a valley appears at $\alpha = 44^\circ$. The directivity patterns for the peak and the valley are plotted in respectively Fig. 11 and Fig. 12. There is no cylinder next to the antenna for these data.

The UE1 is located at an angle of $\theta = \alpha/2$. For the case of the maximum $\theta = 14.5^\circ$ and for the minimum $\theta = 22^\circ$. In Fig. 11, the directivity of UE1 is 6.02 dBi and the directivity of UE2 is -49.44 dBi at $\theta = 14.5^\circ$.

That is a difference of 55.46 dB. The power of the interfering UE is low because it is exactly in between two lobes. Compared to the power of the wanted signal, the received signal power of the interferer is much lower. In Fig. 12, the directivity of UE1 is 6.02 dBi and the directivity of UE2 is -5.33 dBi at $\theta = 22^\circ$. That is a difference of only 11.35 dB. The signal power is approximately the same as in the previous case, but now the interference power is higher. The directivity pattern from the opposite UE has a sidelobe at exactly the angle where the wanted UE is located. When looking at (12), it makes sense the SINR is high in case of $\alpha = 29^\circ$ and low for $\alpha = 44^\circ$.

For comparison, also the directivity patterns when using the zero forcing precoding scheme are plotted. They can be seen in Figs. 13 and 14 for $\alpha = 29^\circ$ and $\alpha = 44^\circ$, respectively. The directivity of the main lobe with ZF precoding is again 6.02 dBi for both values of α , just like the MF case. In contrast with the MF precoding, now the directivity from the UE which is not of interest is forced to zero. For both values of α the directivity of the interferer is 0. The interference power does not play a role when calculating the SINR.

The peaks and valleys of the plots in Fig. 9 shift depending on the simulation scenario and value of the parameters. At some values for α the SINR is improved by at most 21.6 dB with respect to the plot without cylinder when looking at a SNR of 30 dB. When looking at a SNR of -10 dB , the SINR can be improved by at most 0.9 dB because there are no peaks in this region of the plot. Contrary, for some plots the SINR will decrease by maximally 26.7 dB with respect to the simulation without cylinder for SNR=30 dB. When the SNR is -10 dB , the attenuation of the SINR can get up to 7.6 dB. However, the magnitude of the attenuation is dependent on the magnitude of the directivity of the interferer at the angle at which the main beam of the wanted user is directed to. For a higher frequency of 30 GHz, the values of the SINR loss can also be seen in the tables mentioned above. The improvement in SINR can get up to 20.2 dB and the attenuation in SINR can get to 29.5 dB for this frequency of operation.

In Fig. 10 the SINR's are plotted for increasing number of antenna elements. Also, the plots for a ZF precoding scheme can be seen here. As can be seen from Fig. 10a-c, the number of peaks increases with the number of antenna elements for the Matched Filter. There are still minima and maxima, but they occur more frequently. This can be explained by the number of sidelobes which increase when increasing the number of elements. So, with more elements there are more sidelobes which can interfere with the wanted signal. On the other hand, there are also more angles where the directivity goes to zero. At these angles there is no interference and therefore a peak in SINR.

In Fig. 10d-f the SINR for the ZF precoding scheme is shown. For most separation angles the SINR depends linearly on the SNR. The reason for this is that by using zero forcing, the interference from the other UE is always suppressed. The directivity at the angle of interest goes to 0 for the interferer. This can be clearly seen in Figs. 13 and 14. For zero forcing the denominator in (12) becomes 1 so the SINR becomes proportional to the SNR. In Fig. 10d, there is a difference in SINR of approximately 3 dB for $\alpha = 20^\circ$ with respect to other values of α . When the number of elements increases this difference gets smaller and eventually approaches zero. In Fig. 10f, $N = 32$ and the SINR plots are almost the same for every α . There is a small difference in value, but the shape is the same. Only for extremely low values of α the magnitude of the SINR gets lower. When the number of antenna elements increases the ZF scheme is able to null the interferer better and better. Just as the array with a high number of elements is able to direct the beam towards a certain angle accurately, it is also able to null the radiating power of a certain angle.

The minimum and the maximum of the SINR loss at 1 GHz for UE1, and the corresponding α angles at which they occur are summarized in Table VIII and Table IX, for $SNR = -10$ dB and $SNR = 30$ dB, respectively.

The corresponding values of the SINR loss at 30 GHz for UE1, and the corresponding α angles at which they occur are summarized in Table X and Table XI, for $SNR = -10$ dB and $SNR = 30$ dB, respectively.

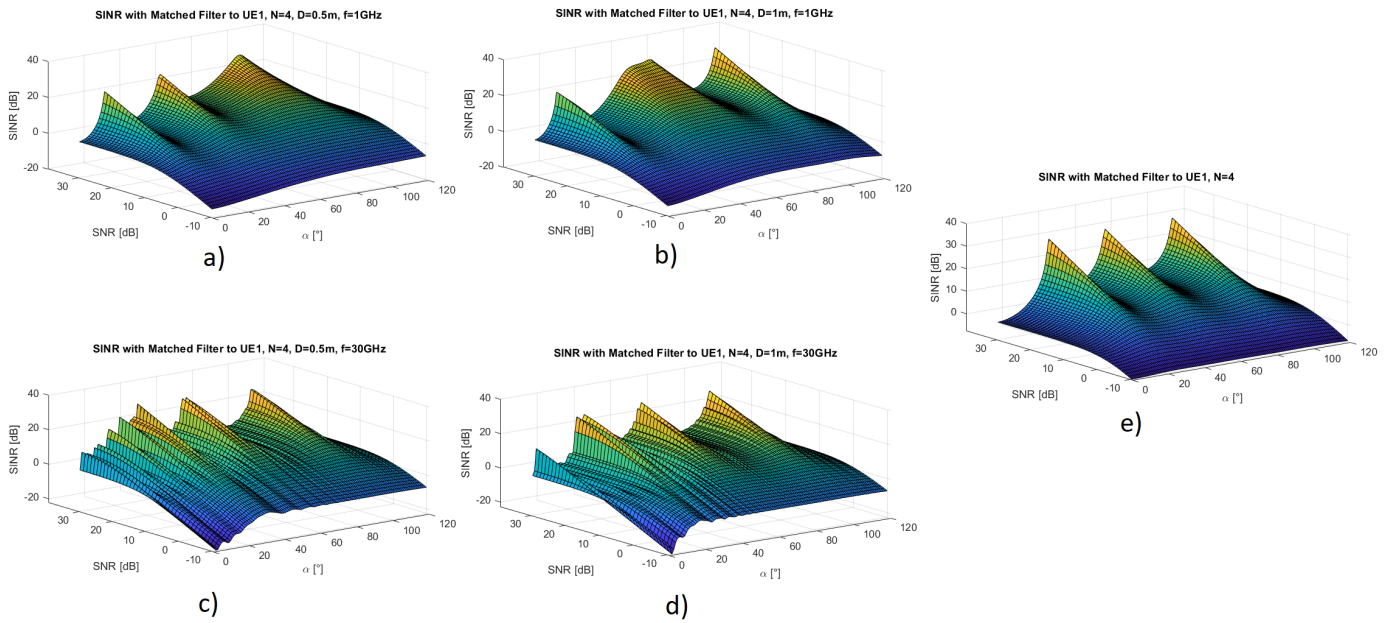


FIG. 9: SINR surface plots for $N=4$ and case I. Plots a) and c) are for $D=0.5$ m. Plots b) and d) are for $D=1$ m. Furthermore, a) and b) are for a frequency of operation of 1 GHz. c) and d) are for $f = 30$ GHz. The last plot, e), is for the case without a cylinder.

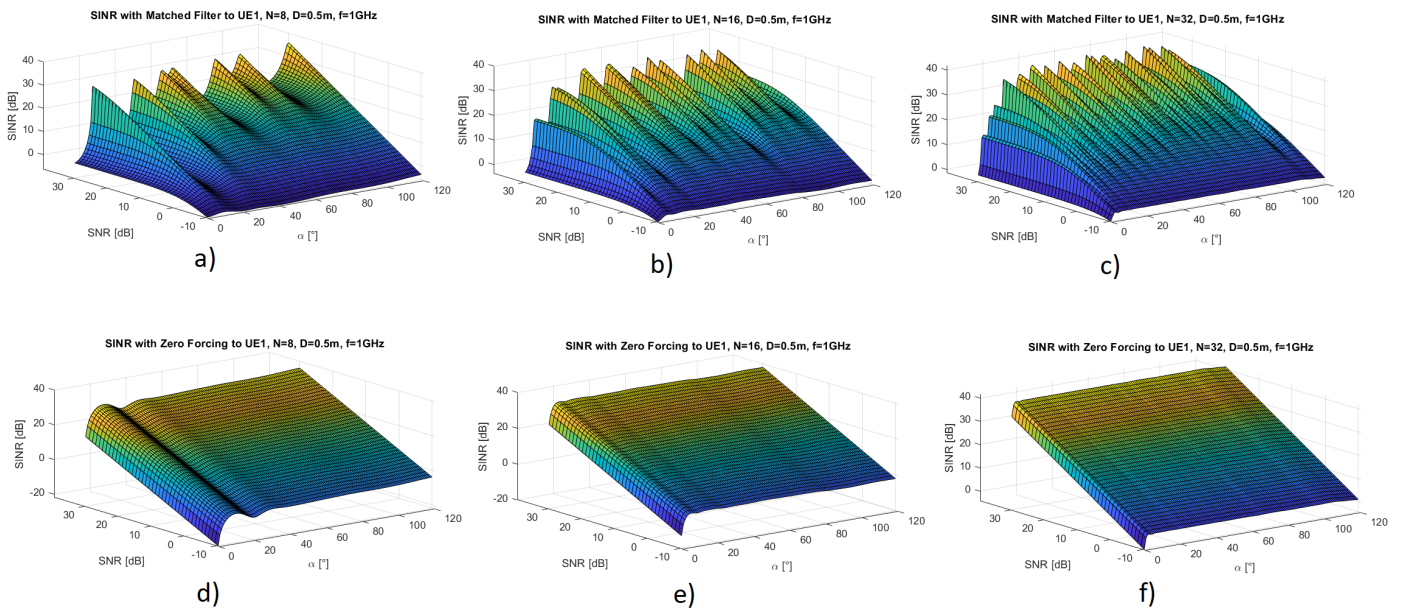


FIG. 10: SINR surface plots for Case I with $f = 1$ GHz and $D=0.5$ m. Plots a)-c) use the MF precoding scheme and plots d)-f) use the ZF precoding scheme. The number of elements increases from left to the right. Plots a) and d) have $N = 8$, plots b) and e) have $N = 16$ and plots c) and f) have $N = 32$.

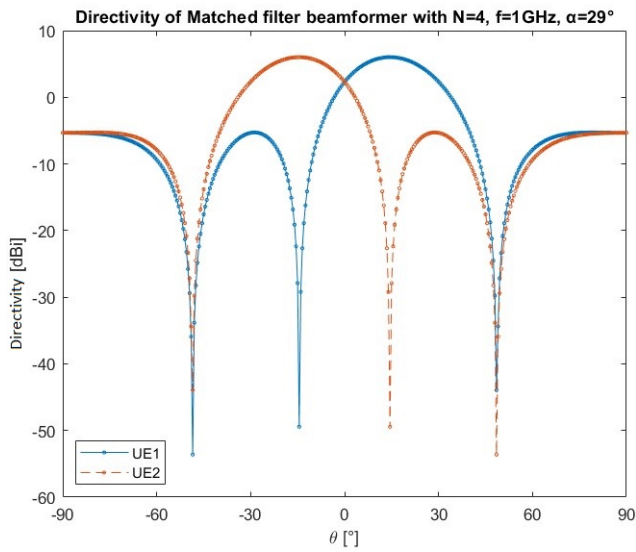


FIG. 11: Matched filter directivity pattern for separation angle α of 29° . Simulated without cylinder.

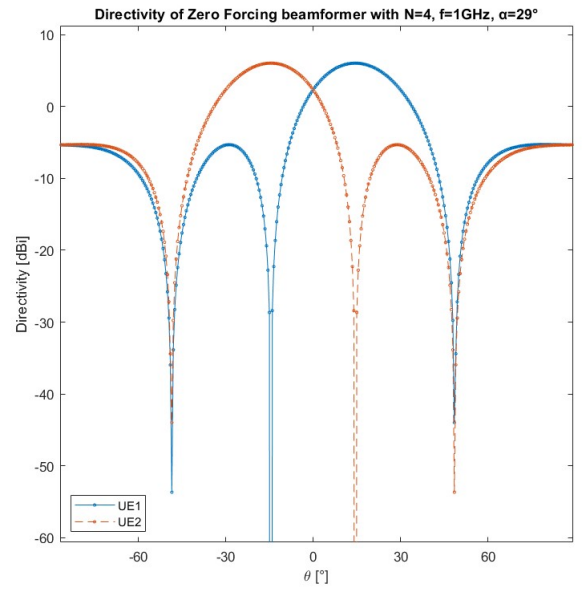


FIG. 13: Zero forcing directivity pattern for separation angle α of 29° . Simulated without cylinder.

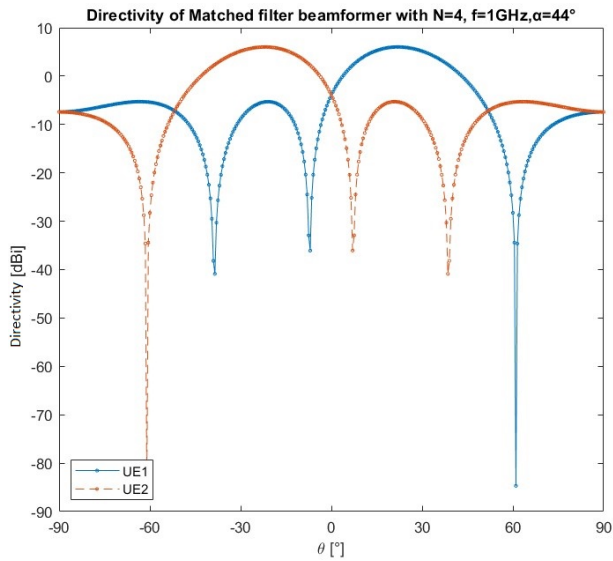


FIG. 12: Matched filter directivity pattern for separation angle α of 44° . Simulated without cylinder.

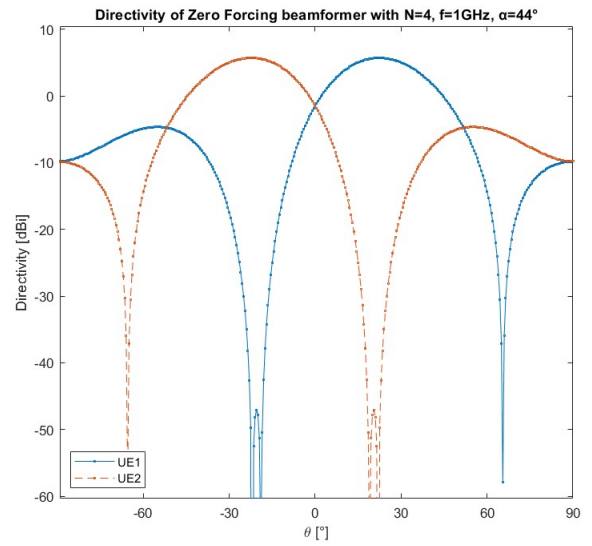


FIG. 14: Zero forcing directivity pattern for separation angle α of 44° . Simulated without cylinder.

TABLE VIII: SINR loss for Case I for $f = 1$ GHz and for $SNR = -10$ dB.

		MF						ZF			
		$L_{\text{SINR,min}}$ [dB]	α_{min} , [°]	$L_{\text{SINR,max}}$ [dB]	α_{max} , [°]			$L_{\text{SINR,min}}$ [dB]	α_{min} , [°]	$L_{\text{SINR,max}}$ [dB]	α_{max} , [°]
N=4	D=0.5 m	-7.6	1	0.6	120	D=0.5 m	-6.8	25	1.5	120	
	D=1 m	-6.9	1	0.9	99	D=1 m	-5.2	23	1.0	76	
N=8	D=0.5 m	-2.4	43	-0.1	120	D=0.5 m	-5.1	21	0.1	1	
	D=1 m	-2.4	17	0.9	107	D=1 m	-4.1	19	1.0	107	
N=16	D=0.5 m	-1.5	95	-0.3	3	D=0.5 m	-1.5	95	-0.1	1	
	D=1 m	-1.2	68	0	120	D=1 m	-1.2	67	0	120	
N=32	D=0.5 m	-1.0	120	0	2	D=0.5 m	-1.0	120	0	1	
	D=1 m	-0.9	108	0	2	D=1 m	-0.9	107	0	1	

TABLE IX: SINR loss for Case I for $f = 1$ GHz and for $SNR = 30$ dB.

		MF						ZF			
		$L_{\text{SINR,min}}$ [dB]	α_{min} , [°]	$L_{\text{SINR,max}}$ [dB]	α_{max} , [°]			$L_{\text{SINR,min}}$ [dB]	α_{min} , [°]	$L_{\text{SINR,max}}$ [dB]	α_{max} , [°]
N=4	D=0.5 m	-26.5	29	21.5	15	D=0.5 m	-6.8	25	1.5	120	
	D=1 m	-26.2	29	21.6	13	D=1 m	-5.2	23	1.0	76	
N=8	D=0.5 m	-26.7	29	20.8	11	D=0.5 m	-5.1	21	0.1	1	
	D=1 m	-21.7	14	18.1	102	D=1 m	-4.1	19	1.0	107	
N=16	D=0.5 m	-21.6	87	16.1	33	D=0.5 m	-1.5	95	-0.1	1	
	D=1 m	-17.7	68	18.2	19	D=1 m	-1.2	67	0	120	
N=32	D=0.5 m	-19.6	115	14.1	31	D=0.5 m	-1.0	120	0	1	
	D=1 m	-16.6	18	15.7	23	D=1 m	-0.9	107	0	1	

TABLE X: SINR loss for Case I for $f = 30$ GHz and for $SNR = -10$ dB.

		MF						ZF			
		$L_{\text{SINR,min}}$ [dB]	α_{min} , [°]	$L_{\text{SINR,max}}$ [dB]	α_{max} , [°]			$L_{\text{SINR,min}}$ [dB]	α_{min} , [°]	$L_{\text{SINR,max}}$ [dB]	α_{max} , [°]
N=4	D=0.5 m	-14.7	3	1.3	32	D=0.5 m	-11.2	7	6.6	1	
	D=1 m	-15.0	3	1.3	19	D=1 m	-6.6	7	4.5	1	
N=8	D=0.5 m	-12.6	1	0.9	34	D=0.5 m	-13.6	7	3.0	1	
	D=1 m	-10.9	3	1.2	19	D=1 m	-7.1	7	3.5	1	
N=16	D=0.5 m	-11.8	4	0.4	38	D=0.5 m	-15.3	3	0.4	38	
	D=1 m	-8.8	1	0.6	20	D=1 m	-12.5	3	0.6	20	
N=32	D=0.5 m	-9.9	3	0.2	44	D=0.5 m	-16.3	3	0.2	44	
	D=1 m	-8.6	3	0.3	26	D=1 m	-12.8	3	0.3	26	

TABLE XI: SINR loss for Case I for $f = 30$ GHz and for $SNR = 30$ dB.

		MF						ZF			
		$L_{\text{SINR,min}}$ [dB]	α_{min} , [°]	$L_{\text{SINR,max}}$ [dB]	α_{max} , [°]			$L_{\text{SINR,min}}$ [dB]	α_{min} , [°]	$L_{\text{SINR,max}}$ [dB]	α_{max} , [°]
N=4	D=0.5 m	-8.8	27	16.9	17	D=0.5 m	-11.2	7	6.6	1	
	D=1 m	-7.0	32	15.7	3	D=1 m	-6.6	7	4.5	1	
N=8	D=0.5 m	-19.6	29	16.1	21	D=0.5 m	-13.6	7	3.0	1	
	D=1 m	-9.7	15	20.2	18	D=1 m	-7.1	7	3.5	1	
N=16	D=0.5 m	-29.5	7	18.2	5	D=0.5 m	-15.3	3	0.4	38	
	D=1 m	-21.1	7	10.7	30	D=1 m	-12.5	3	0.6	20	
N=32	D=0.5 m	-25.8	7	12.5	34	D=0.5 m	-16.3	3	0.2	44	
	D=1 m	-17.9	7	18.4	16	D=1 m	-12.8	3	0.3	26	

2. SINR Case II

Just as for case I, the SINR plots were also made for case II. The difference is that for Case II it is interesting to look at the plot for UE2 as well. Since the waves are not coming in symmetrically anymore, the plots for UE1 and UE2 are not the same. In Fig. 16 the SINR's for the matched filter at a frequency of operation of 1 GHz are plotted. Fig. 17 contains the same plots as Fig. 16, but $f = 30$ GHz.

For $N = 4$ in Figs. 16a and 16b, the received SINR at UE1 improves gradually with increasing angle α . On the other hand, the received SINR gets worse at UE2 for increasing α in Figs. 16d and 16e. Especially for low SNR this pattern is clearly visible. At low values of α the signal from UE1 experiences a relatively high interference from the signal of UE2. When increasing α , the incoming angle for UE1 gets higher and moves away from the incoming wave from UE2. Less interference is experienced. Contrary, when having a low α the SINR of UE2 is at its highest. This is because this wave is coming in at broadside, on the other side of the cylinder. At low α both incoming waves are blocked by the cylinder. However, when increasing α the incoming wave of UE1 gets the chance to reach the ULA without getting blocked by the cylinder. Therefore, more interference from UE1 is coming in when the signal from UE2 is the wanted signal. This is why there is a decreasing line in α vs. SINR for UE2.

At high SNR this relation does not hold. There is a peak in SINR at a certain values for α , depending on D . For example, for $D = 1$ m (Fig. 16b and e) there is a maximum around $\alpha = 30^\circ$. The SINR for case I, $N = 4$ and without the cylinder can be seen in Fig. 15. In this plot there is a peak around $\alpha = 30^\circ$ as well. This appears to be a separation angle for $N = 4$ where the SINR is high. The cylinder has no influence on this. It is caused by the properties of the ULA itself.

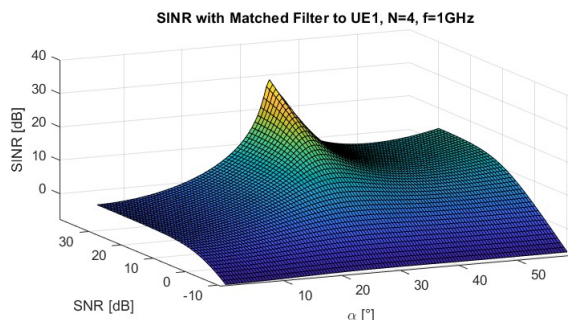


FIG. 15: SINR plot for Case I with $N = 4$ and $f = 1$ GHz. This plot was made for a simulation without cylinder.

Furthermore, the SINR plots when $N = 32$ and

$f = 1$ GHz look exactly the same for both UE's. This can be seen when comparing Fig. 16c and f. For an increasing number of elements, the plots for UE1 and UE2 are looking more and more alike when considering a lower frequency. The size of the antenna gets bigger with more elements. This makes the cylinder relatively small. When there is no cylinder, both plots are the same because the power of a plane wave is the same everywhere. So when the size of the ULA becomes bigger, the cylinder plays a smaller role and the situation approaches free space line-of-sight situation.

Contrary, when having a frequency of 30 GHz as in Fig. 17, the plots for both UE's always look different. The reason is the frequency of operation. The cylinder now does play a role because at the frequency of operation the size of the ULA is not as big as when having $f = 1$ GHz. The cylinder blocking the incoming waves has an impact on the SINR plots. Moreover, When having $N = 32$ like in Fig. 17c and f, at low SNR the SINR is increasing with α for UE1 and decreasing with α for UE2. This is for the same reason as mentioned earlier for Fig. 16a and 16d. In these plots, exactly the same behavior was seen.

Apart from the difference at low values of α , the Fig. 17a, b, d and e look similar to the Fig. 16a, b, d and e. The change in frequency does not have a lot of influence on what the SINR looks like when having $N = 4$. Again what comes back is the maximum in SINR at a separation angle of around 30° .

The minimum and the maximum of the SINR loss at 1 GHz for UE1, and the corresponding α angles at which they occur are summarized in Table XII and Table XIII, for $SNR = -10$ dB and $SNR = 30$ dB, respectively.

The corresponding values of the SINR loss at 30 GHz for UE1, and the corresponding α angles at which they occur are summarized in Table XIV and Table XV, for $SNR = -10$ dB and $SNR = 30$ dB, respectively.

The minimum and the maximum of the SINR loss at 1 GHz for UE2, and the corresponding α angles at which they occur are summarized in Table XVI and Table XVII, for $SNR = -10$ dB and $SNR = 30$ dB, respectively.

The corresponding values of the SINR loss at 30 GHz for UE2, and the corresponding α angles at which they occur are summarized in Table XVIII and Table XIX, for $SNR = -10$ dB and $SNR = 30$ dB, respectively.

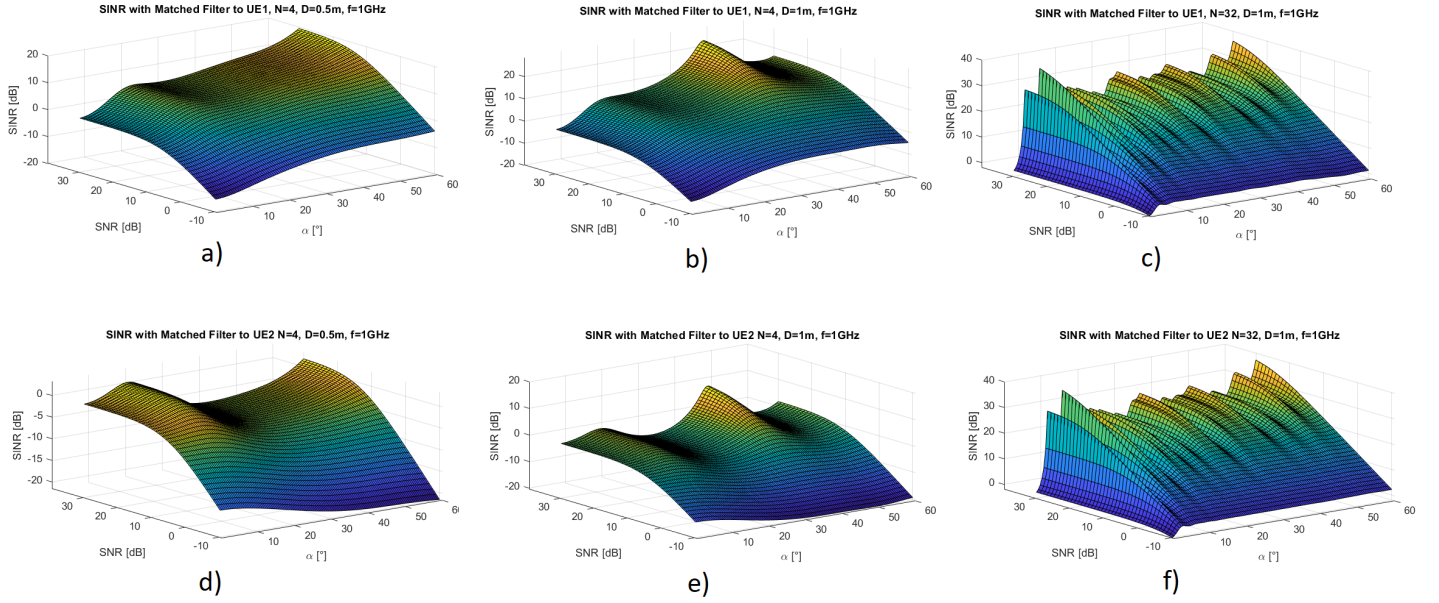


FIG. 16: SINR surface plots for $f = 1$ GHz with use of MF beamformer. Plots a)-c) are for UE1 and plots d)-f) are for UE2. Plots a) and d) are for $D = 0.5$ m and $N = 4$. Plots b) and e) are for $D = 1$ m and $N = 4$. Lastly, plots c) and f) are for $D = 1$ m and $N = 32$.

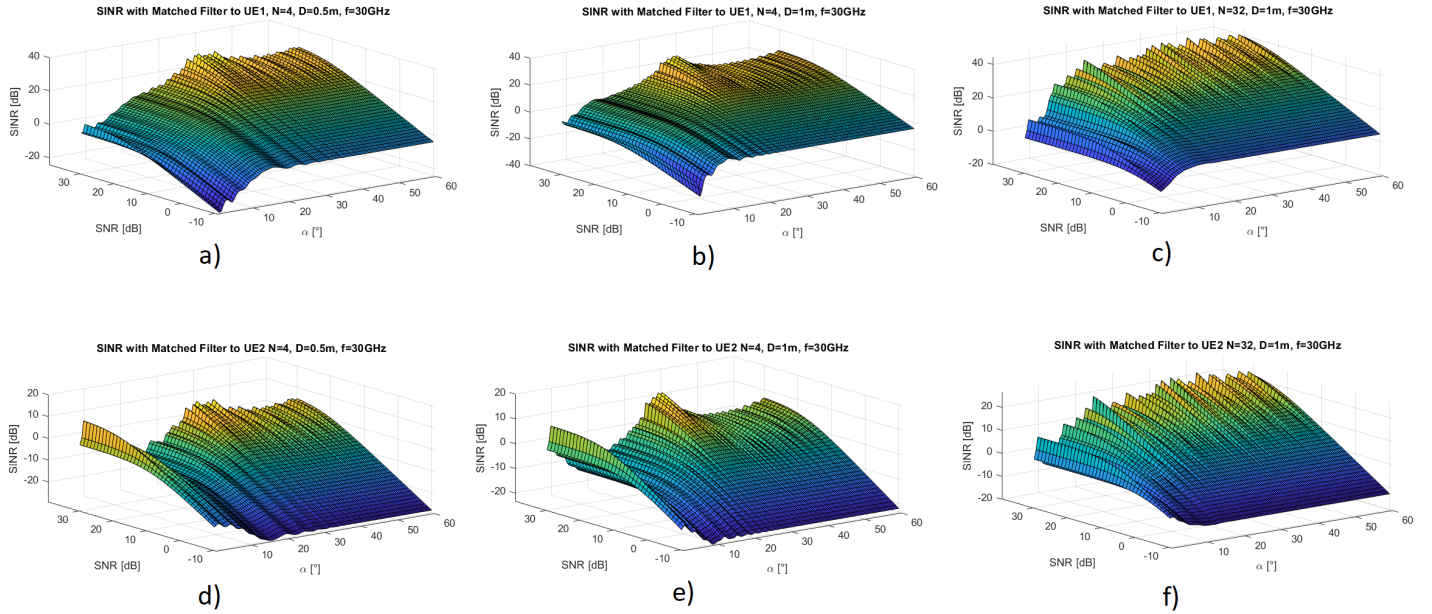


FIG. 17: SINR surface plots for $f = 30$ GHz with use of MF beamformer. Plots a)-c) are for UE1 and plots d)-f) are for UE2. Plots a) and d) are for $D = 0.5$ m and $N = 4$. Plots b) and e) are for $D = 1$ m and $N = 4$. Lastly, plots c) and f) are for $D = 1$ m and $N = 32$.

TABLE XII: SINR loss for UE1 in Case II for $f = 1$ GHz and for $SNR = -10$ dB.

		MF				ZF				
		$L_{\text{SINR,min}}$ [dB]	α_{min} , [°]	$L_{\text{SINR,max}}$ [dB]	α_{max} , [°]	$L_{\text{SINR,min}}$ [dB]	α_{min} , [°]	$L_{\text{SINR,max}}$ [dB]	α_{max} , [°]	
N=4	D=0.5 m	-7.6	0.5	2.9	60	D=0.5 m	-9.7	28.5	-2.8	0.5
	D=1 m	-6.9	0.5	3.4	48.5	D=1 m	-7.0	24	-0.9	0.5
N=8	D=0.5 m	-3.4	20.5	0.4	60	D=0.5 m	-3.7	19.5	0.1	0.5
	D=1 m	-1.9	14.5	2.1	53	D=1 m	-4.0	17	-0.6	0.5
N=16	D=0.5 m	-2.0	47	-0.1	4.5	D=0.5 m	-1.1	47	0	0.5
	D=1 m	-1.5	34.5	0.3	60	D=1 m	-1.1	10	0	0.5
N=32	D=0.5 m	-1.5	60	0	1.5	D=0.5 m	-0.6	60	0	0.5
	D=1 m	-1.3	53.5	-0.1	1.5	D=1 m	-0.6	53.5	0	0.5

TABLE XIII: SINR loss for UE1 in Case II for $f = 1$ GHz and for $SNR = 30$ dB.

		MF				ZF				
		$L_{\text{SINR,min}}$ [dB]	α_{min} , [°]	$L_{\text{SINR,max}}$ [dB]	α_{max} , [°]	$L_{\text{SINR,min}}$ [dB]	α_{min} , [°]	$L_{\text{SINR,max}}$ [dB]	α_{max} , [°]	
N=4	D=0.5 m	-23.8	30	5.6	13	D=0.5 m	-9.7	28.5	-2.8	0.5
	D=1 m	-18.7	30	16.3	41	D=1 m	-7.0	24	-0.9	0.5
N=8	D=0.5 m	-29.0	14.5	5.3	57	D=0.5 m	-3.7	19.5	0.1	0.5
	D=1 m	-30.2	14.5	2.2	8.5	D=1 m	-4.0	17	-0.6	0.5
N=16	D=0.5 m	-22.2	14.5	18.1	6.5	D=0.5 m	-1.1	47	0	0.5
	D=1 m	-22.3	22	6.8	6	D=1 m	-1.1	10	0	0.5
N=32	D=0.5 m	-17.8	54.5	9.1	10.5	D=0.5 m	-0.6	60	0	0.5
	D=1 m	-16.8	30	11.0	7.5	D=1 m	-0.6	53.5	0	0.5

TABLE XIV: SINR loss for UE1 in Case II for $f = 30$ GHz and for $SNR = -10$ dB.

		MF				ZF				
		$L_{\text{SINR,min}}$ [dB]	α_{min} , [°]	$L_{\text{SINR,max}}$ [dB]	α_{max} , [°]	$L_{\text{SINR,min}}$ [dB]	α_{min} , [°]	$L_{\text{SINR,max}}$ [dB]	α_{max} , [°]	
N=4	D=0.5 m	-16.7	1.5	4.3	16	D=0.5 m	-11.8	3.5	7.3	0.5
	D=1 m	-19.8	1.5	4.5	9	D=1 m	-8.0	3.5	5.2	1
N=8	D=0.5 m	-12.4	0.5	3.7	17	D=0.5 m	-14.7	3.5	4.1	0.5
	D=1 m	-12.1	1.5	4.0	9.5	D=1 m	-8.9	3.5	4.2	0.5
N=16	D=0.5 m	-11.0	1.5	3.2	19	D=0.5 m	-18.9	3.5	-2.3	0.5
	D=1 m	-8.6	0.5	3.4	10	D=1 m	-12.0	3	1.2	0.5
N=32	D=0.5 m	-8.3	3	2.9	22	D=0.5 m	-16.4	3	-4.5	0.5
	D=1 m	-5.5	0.5	2.9	12.5	D=1 m	-12.7	3	-3.2	0.5

TABLE XV: SINR loss for UE1 in Case II for $f = 30$ GHz and for $SNR = 30$ dB.

		MF				ZF				
		$L_{\text{SINR,min}}$ [dB]	α_{min} , [°]	$L_{\text{SINR,max}}$ [dB]	α_{max} , [°]	$L_{\text{SINR,min}}$ [dB]	α_{min} , [°]	$L_{\text{SINR,max}}$ [dB]	α_{max} , [°]	
N=4	D=0.5 m	-4.2	30	20.4	37	D=0.5 m	-11.8	3.5	7.3	0.5
	D=1 m	-3.8	1.5	11.1	38	D=1 m	-8.0	3.5	5.2	1
N=8	D=0.5 m	-15.0	14.5	21.5	25.5	D=0.5 m	-14.7	3.5	4.1	0.5
	D=1 m	-9.7	14.5	19.0	17.5	D=1 m	-8.9	3.5	4.2	0.5
N=16	D=0.5 m	-24.0	7	17.6	25.5	D=0.5 m	-18.9	3.5	-2.3	0.5
	D=1 m	-15.3	7	22.9	12	D=1 m	-12.0	3	1.2	0.5
N=32	D=0.5 m	-28.4	3.5	16.9	21	D=0.5 m	-16.4	3	-4.5	0.5
	D=1 m	-25.6	3.5	18.8	16.5	D=1 m	-12.7	3	-3.2	0.5

TABLE XVI: SINR loss for UE2 in Case II for $f = 1$ GHz and for $SNR = -10$ dB.

		MF				ZF				
		$L_{\text{SINR,min}}$ [dB]	α_{min} , [°]	$L_{\text{SINR,max}}$ [dB]	α_{max} , [°]	$L_{\text{SINR,min}}$ [dB]	α_{min} , [°]	$L_{\text{SINR,max}}$ [dB]	α_{max} , [°]	
N=4	D=0.5 m	-14.6	60	-7.7	0.5	D=0.5 m	-9.7	28.5	-2.8	0.5
	D=1 m	-13.5	49.5	-6.9	0.5	D=1 m	-7.0	24	-0.9	0.5
N=8	D=0.5 m	-1.7	60	-0.7	26	D=0.5 m	-3.7	19.5	0.1	0.5
	D=1 m	-4.3	53.5	-1.8	0.5	D=1 m	-4.0	17	-0.6	0.5
N=16	D=0.5 m	-1.0	10	-0.2	47	D=0.5 m	-1.1	47	0	0.5
	D=1 m	-0.9	60	-0.3	3.5	D=1 m	-1.1	10	0	0.5
N=32	D=0.5 m	-0.2	5	0.3	60	D=0.5 m	-0.6	60	0	0.5
	D=1 m	-0.3	5	0.2	53.5	D=1 m	-0.6	53.5	0	0.5

TABLE XVII: SINR loss for UE2 in Case II for $f = 1$ GHz and for $SNR = 30$ dB.

		MF				ZF				
		$L_{\text{SINR,min}}$ [dB]	α_{min} , [°]	$L_{\text{SINR,max}}$ [dB]	α_{max} , [°]	$L_{\text{SINR,min}}$ [dB]	α_{min} , [°]	$L_{\text{SINR,max}}$ [dB]	α_{max} , [°]	
N=4	D=0.5 m	-37.2	30	1.2	10	D=0.5 m	-9.7	28.5	-2.8	0.5
	D=1 m	-34.5	30	1.3	9.5	D=1 m	-7.0	24	-0.9	0.5
N=8	D=0.5 m	-27.2	14.5	5.9	10.5	D=0.5 m	-3.7	19.5	0.1	0.5
	D=1 m	-31.1	14.5	1.8	8	D=1 m	-4.0	17	-0.6	0.5
N=16	D=0.5 m	-22.2	14.5	17.7	6.5	D=0.5 m	-1.1	47	0	0.5
	D=1 m	-21.9	22	6.9	6	D=1 m	-1.1	10	0	0.5
N=32	D=0.5 m	-17.4	54.5	9.2	10.5	D=0.5 m	-0.6	60	0	0.5
	D=1 m	-16.6	30	11.0	7.5	D=1 m	-0.6	53.5	0	0.5

TABLE XVIII: SINR loss for UE2 in Case II for $f = 30$ GHz and for $SNR = -10$ dB.

		MF				ZF				
		$L_{\text{SINR,min}}$ [dB]	α_{min} , [°]	$L_{\text{SINR,max}}$ [dB]	α_{max} , [°]	$L_{\text{SINR,min}}$ [dB]	α_{min} , [°]	$L_{\text{SINR,max}}$ [dB]	α_{max} , [°]	
N=4	D=0.5 m	-22.1	16	-9.8	1.5	D=0.5 m	-11.8	3.5	7.3	0.5
	D=1 m	-15.9	9	-5.7	1.5	D=1 m	-8.0	3.5	5.2	1
N=8	D=0.5 m	-26.9	16.5	-13.3	0.5	D=0.5 m	-14.7	3.5	4.1	0.5
	D=1 m	-17.9	9.5	-7.4	1.5	D=1 m	-8.9	3.5	4.2	0.5
N=16	D=0.5 m	-22.3	19.5	-9.8	1	D=0.5 m	-18.9	3.5	-2.3	0.5
	D=1 m	-21.3	9.5	-9.7	0.5	D=1 m	-12.0	3	1.2	0.5
N=32	D=0.5 m	-18.4	22	-6.9	0.5	D=0.5 m	-16.4	3	-4.5	0.5
	D=1 m	-15.4	13	-5.5	0.5	D=1 m	-12.7	3	-3.2	0.5

TABLE XIX: SINR loss for UE2 in Case II for $f = 30$ GHz and for $SNR = 30$ dB.

		MF				ZF				
		$L_{\text{SINR,min}}$ [dB]	α_{min} , [°]	$L_{\text{SINR,max}}$ [dB]	α_{max} , [°]	$L_{\text{SINR,min}}$ [dB]	α_{min} , [°]	$L_{\text{SINR,max}}$ [dB]	α_{max} , [°]	
N=4	D=0.5 m	-28.1	30	11.6	1.5	D=0.5 m	-11.8	3.5	7.3	0.5
	D=1 m	-20.8	30	10.3	1.5	D=1 m	-8.0	3.5	5.2	1
N=8	D=0.5 m	-44.9	14.5	11.2	1.5	D=0.5 m	-14.7	3.5	4.1	0.5
	D=1 m	-29.9	14.5	10.5	1.5	D=1 m	-8.9	3.5	4.2	0.5
N=16	D=0.5 m	-38.4	14.5	11.3	1.5	D=0.5 m	-18.9	3.5	-2.3	0.5
	D=1 m	-36.8	7	9.5	1.5	D=1 m	-12.0	3	1.2	0.5
N=32	D=0.5 m	-35.1	14.5	9.9	1.5	D=0.5 m	-16.4	3	-4.5	0.5
	D=1 m	-32.9	3.5	7.8504	1.5	D=1 m	-12.7	3	-3.2	0.5

IV. CONCLUSION

To conclude, the blockage impact of a cylinder on the beamforming performance of the ideal matched filter and the zero forcing precoding schemes depends on the number of antenna elements, the frequency of operation and the separation distance between cylinder and array antenna. Both beamforming algorithms adapt to the scattered field by the cylinder emulating the human body. We have considered a multi-user scenario with 2 users.

By increasing the number of antenna elements, the beamwidth gets lower and the magnitude of the directivity increases since it is equal to the number of elements, $D_{ant,max} = N$. In the presence of a cylinder, the attenuation of the directivity of the main beam at $N = 4$ can go up to 1.85 dB for the MF precoder and 3.4 dB for the ZF precoder at a frequency of operation of 1 GHz. By increasing the number of elements to 32, the attenuation is 1.6 dB and 0.5 for the MF and ZF precoding schemes at 1 GHz, respectively. Furthermore, the direction of the main beam is pointed more accurately towards the desired UE when having a high number of antenna elements. For example, with $N = 4$ in case I, the main beam is often pointed to a direction other than $\theta = \pm\alpha/2$ when $\alpha < 80^\circ$. For $N = 32$ the main beam is always located at $\theta = \pm\alpha/2$ for every value of α .

If the ZF precoding scheme is used, the SINR can potentially be improved by approximately 6 dB by increasing the number of elements in the array because the antenna is able to more accurately null the interferer. When using the MF precoding scheme, the number of peaks in the SINR increases. The SINR is improved at specific values for the separation angles, depending on the number of elements. The SINR can improve by approximately 20 dB. On the other hand, the SINR can also become worse since it can also decrease by approximately 30 dB.

By increasing the frequency of operation, the size of the array goes down because the inter-element distance is dependent on the wavelength. For $N = 4$, the directivity of the main beam goes from 4.3 dBi to 5.9 dBi when increasing the frequency from 1 GHz to 30 GHz. For $N = 32$, the directivity was attenuated by maximally ± 10 dB at angles $\alpha < 30^\circ$ when going from 1 GHz to 30 GHz. Therefore, when using $N = 4$ the increase in frequency improves the directivity, while for $N = 32$ it decreases the directivity.

The frequency of operation can also have influence on the received SINR when using the MF precoder. The size of the array goes down with a higher frequency, so then the cylinder becomes relatively bigger. The array can be hidden behind the cylinder. Depending on the angles of the incoming waves, the SINR can either

improve or deteriorate by a maximum of 20 dB. For example, when the interferer is coming in at broadside at $f = 30$ GHz, the array is hidden and there is not a lot of interference. Contrary, when the desired signal is coming in at broadside, the SINR becomes worse since this signal power is blocked.

The separation distance between the cylinder and the ULA has significant impact on the performance of the antenna. The improvement in directivity when changing the distance $D = 0.5$ m to $D = 1.0$ can go up to 10 dB for certain angles α . The range of incoming angles α for which the directivity is attenuated is extended by up to 15° when locating the cylinder 0.5 m closer to the antenna. Moreover, in most cases when the cylinder is located closer to the antenna, the sidelobe magnitudes are higher. For example, when going from $D = 1$ m to $D = 0.5$ m when the wave is coming in at broadside for the MF, the sidelobes are increased by 6.5 dB for $N = 4$ at 1 GHz.

Only at a small number of antenna elements (e.g. $N = 4$) and at a frequency of 1 GHz, the separation distance also has influence on the received SINR if the MF precoder is used. At high SNR, peaks in the SINR appear at different separation angles when the array is located further away from the cylinder. Where first a valley was located, now a peak is located, so this can be a maximum improvement of around 20 dB as well.

REFERENCES

- [1] M. Ali Babar Abbasi and Vincent F. Fusco, "Beamformer development challenges for 5G and beyond," *Antennas and Propagation for 5G and Beyond*, pp. 265–299, 2020. [Online]. Available: <https://doi.org/10.1049/PBTE093E.ch>
- [2] U. T. Virk and K. Haneda, "Modeling Human Blockage at 5G Millimeter-Wave Frequencies," *IEEE Transactions on Antennas and Propagation*, vol. 68, no. 3, pp. 2256–2266, 3 2020.
- [3] M. Ghaddar, L. Talbi, T. A. Denidni, and A. Sebak, "A conducting cylinder for modeling human body presence in indoor propagation channel," *IEEE Transactions on Antennas and Propagation*, vol. 55, no. 11 I, pp. 3099–3103, 11 2007.
- [4] I. L. Rozeboom, "Beamforming Performance Evaluation with Impact of User Model Electric Properties," University of Twente, Enschede, Tech. Rep.
- [5] A. A. Glazunov, "Downlink Massive MIMO performance of a vertically polarized uniform linear array in Random Line-Of-Sight," in *2016 10th European Conference on Antennas and Propagation, EuCAP 2016*. Institute of Electrical and Electronics Engineers Inc., 5 2016.
- [6] R. F. Harrington, *Time-Harmonic Electromagnetic Fields*, D. G. Dudley, Ed. Wiley-IEEE Press, 2001.
- [7] G. Kevin Zhu, "Cylinder scattering," 2011. [Online]. Available: <https://nl.mathworks.com/matlabcentral/fileexchange/30162-cylinder-scattering>

- [8] E. Björnson, J. Hoydis, and L. Sanguinetti, “Massive MIMO networks: Spectral, energy, and hardware efficiency,” pp. 154–655, 2017. [Online]. Available: <https://massivemimobook.com/>
- [9] X. Gao, L. Dai, Z. Gao, T. Xie, and Z. Wang, “Precoding for mmWave massive MIMO,” in *mmWave Massive MIMO: A Paradigm for 5G*. Elsevier Inc., 2017, pp. 79–111.
- [10] C. A. Balanis, *Antenna Theory: Analysis and Design, (3RD ED.)*. John Wiley & Sons Inc., 2009.
- [11] S. V. Hum, “Radio and Microwave Wireless Systems Course Notes,” 2018. [Online]. Available: <https://www.waves.utoronto.ca/prof/svhum/ece422.html>